Data-driven study of the implications of anomalous magnetic moments and lepton flavor violating processes of e, μ, and τ

Chun-Khiang Chua◉

Department of Physics and Center for High Energy Physics Chung Yuan Christian University Chung-Li,
Taiwan 320, Republic of China

We study anomalous magnetic moments and flavor violating processes of e, μ, and τ leptons. We use a data driven approach to investigate the implications of the present data on the parameters of a class of models, which has spin-0 scalar and spin-1/2 fermion fields. We compare two different cases, which has or does not have a built-in cancelation mechanism. Our findings are as following. Chiral interactions are unable to generate large enough Δa_e and Δa_μ to accommodate the experimental results. Although sizable Δa_e and Δa_μ can be generated from nonchiral interactions, they are not contributed from the same source. Presently, the upper limit of $\mu \to e\gamma$ decay gives the most severe constraints on photonic penguin contributions in $\mu \to e$ transitions, but the situation may change in considering future experimental sensitivities. The Z-penguin diagrams can constrain chiral interaction better than photonic penguin diagrams in $\mu \to e$ transitions. In most of the parameter space, box contributions to $\mu \to 3e$ decay are subleading. The present bounds on Δa_τ and d_τ are unable to give useful constraints on parameters. In $\tau \to e$ (μ) transitions, the present $\tau \to e\gamma$ ($\mu\gamma$) upper limit constrains the photonic penguin contribution better than the $\tau \to 3e$ (3μ) upper limit, and Z-penguin amplitudes constrain chiral interaction better than photonic penguin amplitudes. Box contributions to $\tau \to 3e$ and $\tau \to 3\mu$ decays can sometime be comparable to Z-penguin contributions. The $\tau^- \to e^-\mu^+e^-$ and $\tau^- \to \mu^-e^+\mu^-$ rates are highly constrained by $\tau \to e\gamma$, $\mu \to e\gamma$ and $\tau \to \mu\gamma$, $\mu \to e\gamma$ upper limits, respectively. We compare the current experimental upper limits, future sensitivities and bounds from consistency on various muon and tau LFV processes.

I. INTRODUCTION

The Large Hadron Collider completed run-2 in 2018 and is currently preparing for run-3. From the results of the searches, we see that new physics (NP) signal is yet to be found (see, for example [1], for a summery of the recent search results). It is therefore useful and timely to explore the high-precision frontier, where the NP at the scale beyond our reach may manifest in low energy processes via virtual effects. Indeed, there are some interesting experimental activities in the lepton sector in recent years.

The muon's anomalous magnetic moment remains as a hint of contributions from NP since 2001 [2]. Presently the deviation of the experimental result $a_\mu^{\rm exp}$ from the Standard Model (SM) expectation $a_\mu^{\rm SM}$ is 3.7σ [3–5]:

$$\Delta a_\mu = a_\mu^{\rm exp} - a_\mu^{\rm SM} = (27.06 \pm 7.26) \pm 10^{-10}. \quad (1)$$

For more details, see [6–9]. New experiments in Fermilab and J-PARC are on their way to improve the sensitivities [10].

In addition, in 2018, a measurements of the fine-structure constant α using the recoil frequency of cesium-133 atoms in a matter-wave interferometer, infered a deviation on electron $g - 2$ from the SM prediction, [11]

$$\Delta a_e = a_e^{\rm exp} - a_e^{\rm SM} = (-0.88 \pm 0.36) \pm 10^{-12}. \quad (2)$$

In the tau sector, the experimental and the theoretical results of the anomalous magnetic moment are given by

$$-0.052 < a_\tau^{\rm exp} < 0.013,$$
$$a_\tau^{\rm SM} = (1.17721 \pm 0.00005) \times 10^{-3}, \quad (3)$$

respectively [4,12]. The experimental sensitivity is roughly one order of magnitude from the SM prediction.

Furthermore, it is known that the SM contributions to lepton electric dipole moments are at four-loop level and, consequently, are highly suppressed. For example, the electron electric dipole moment was estimated to be $d_e \simeq 8 \times 10^{-41}$ e cm [13]. The present experimental

bounds on electric dipole moment of e, μ, and τ are given by [14,15]

$$|d_e| < 1.1 \times 10^{-29} \text{ e cm}, \tag{4}$$

$$|d_\mu| < 1.9 \times 10^{-19} \text{ e cm}, \tag{5}$$

and

$$|d_\tau| < 1.6 \times 10^{-18} \text{ e cm}, \tag{6}$$

where the above limit on d_e is used to constrain d_τ via $\Delta d_e = 6.9 \times 10^{-12} d_\tau$ [16].

It is known that SM prohibits charge lepton flavor violating (LFV) processes. Hence, they are excellent probes of NP. Indeed, they are under intensive searches. In 2016 the MEG collaboration reported the search result of $\mu \to e\gamma$ decay, [17]

$$\mathcal{B}(\mu^+ \to e^+ \gamma) \leq 4.2 \times 10^{-13}, \tag{7}$$

and the upgrade is on the way to improve the sensitivity by roughly one order of magnitude [18]. Interestingly, $\mu \to e\gamma$ decay may be closely related to lepton anomalous magnetic moments and other LFV processes, such as $\mu^+ \to 3e$ decays and muon to electron conversions, $\mu^- N \to e^- N$ [19]. See [20] for a review on $(g-2)_\mu$ and LFV processes. Note that LFV processes can sometime be related to cosmological effects, see for example [21].

Lepton flavor violating τ decays are also under intensive search. Current bounds on $\tau \to e\gamma$, $\mu\gamma$, $3e$, 3μ, $e\bar{\mu}e$, $\mu\bar{e}\mu$ decays was provided by B factories. They are at the level of 10^{-8} and the sensitivities will be improved by two orders of magnitude in the updated B factory [22,23].

The current limits and future experimental sensitivities of various $l' \to l\gamma$, $l \to l'\bar{l}''l'$, and $lN \to l'N$ processes are summarized in Table I.

TABLE I. Present upper limits and future sensitivities of some muon and tau lepton flavor violating processes are listed [4,17,18,22–24].

	Current limit	Future sensitivity
$\mathcal{B}(\mu^+ \to e^+\gamma)$	$<4.2 \times 10^{-13}$	6×10^{-14}
$\mathcal{B}(\mu^+ \to e^+e^+e^-)$	$<1.0 \times 10^{-12}$	10^{-16}
$\mathcal{B}(\mu^- \text{Ti} \to e^- \text{Ti})$	$<4.3 \times 10^{-12}$	10^{-17}
$\mathcal{B}(\mu^- \text{Au} \to e^- \text{Au})$	$<7 \times 10^{-13}$	10^{-16}
$\mathcal{B}(\mu^- \text{Al} \to e^- \text{Al})$	$\cdots$	10^{-17}
$\mathcal{B}(\tau^- \to e^-\gamma)$	$<3.3 \times 10^{-8}$	3×10^{-9}
$\mathcal{B}(\tau^- \to \mu^-\gamma)$	$<4.4 \times 10^{-8}$	1×10^{-9}
$\mathcal{B}(\tau^- \to e^-e^+e^-)$	$<2.7 \times 10^{-8}$	4.3×10^{-10}
$\mathcal{B}(\tau^- \to \mu^-e^+\mu^-)$	$<1.7 \times 10^{-8}$	2.7×10^{-10}
$\mathcal{B}(\tau^- \to e^-\mu^+e^-)$	$<1.5 \times 10^{-8}$	2.4×10^{-10}
$\mathcal{B}(\tau^- \to \mu^-\mu^+\mu^-)$	$<2.1 \times 10^{-8}$	3.3×10^{-10}

Many popular NP scenarios or models are disfavored or even closed to being ruled out by data (see, for example, [1]). Given the present situation, it is worthy to use a data driven approach. It will be interesting to see where the present data lead us to. As a working assumption, we consider a general class of models that lepton anomalous magnetic moment and various lepton flavor violating processes, such as $\mu \to e\gamma$, $\mu \to 3e$, $\mu \to e$ conversions, $\tau \to e\gamma$, $\mu\gamma$, $3e$, 3μ, $e\bar{\mu}e$, and $\mu\bar{e}\mu$ decays are induced by loop diagrams via exchanging spin-0 and spin-1/2 particles in this work.

Note that the above mentioned experimental results of Δa_μ and Δa_e received a lot of attention. There are studies involving leptoquark, two Higgs doublets, supersymmetry particles, dark matters and so on [25–78]. It is interesting that many new physics models in these studies are similar to the framework adopted here. Furthermore, by considering simultaneously various processes or quantities involving different leptons, one can obtain useful information on new physics. For example, in [27] by using effective field theory (EFT) and some simplified models similar to the present framework, the authors found that the $\mu \to e\gamma$ bound requires the muon and electron sectors to be decoupled and, consequently, Δa_μ and Δa_e cannot be explained from the same source, but as a bonus a large muon electric dipole moment is possible. In addition, it is known in the literature that there are relations on $l' \to l\bar{l}''l'''$ and $l' \to l\gamma$ rates. For example, using an EFT approach [79,80], $l' \to l\bar{l}l$ and $l' \to l\gamma$ rates are shown to be related as following,

$$\mathcal{B}(\mu \to 3e) \simeq \frac{1}{160} \mathcal{B}(\mu \to e\gamma),$$

$$\mathcal{B}(\tau \to 3e) \simeq \frac{1}{95} \mathcal{B}(\tau \to e\gamma),$$

$$\mathcal{B}(\tau \to 3\mu) \simeq \frac{1}{440} \mathcal{B}(\tau \to \mu\gamma), \tag{8}$$

if the photonic dipole penguins dominate in these $l' \to l\bar{l}l$ decays. It is also known that the constraints on 4-lepton and Z-lepton-lepton contributions using $l' \to l\bar{l}l$ bounds are found to be less severe than the constraints of γ-lepton-lepton contributions using $l' \to l\gamma$ bounds [80]. Studies involving different processes are useful to search for NP and to probe its properties as well.

It will be useful to compare the present approach to an EFT approach (see, for example, [27,80,81]). For illustration, we use the above mentioned analysis on Δa_μ, Δa_e, and the $\mu \to e\gamma$ decay as an example. As stated in [27], the relevant effective Hamiltonian is

$$H_{\text{eff}} = c_R^{l_f l_i} \bar{l}_f \sigma_{\mu\nu} P_R l_i F^{\mu\nu} + \text{H.c.}, \tag{9}$$

giving

$$a_{l_i} = -\frac{4m_{l_i}}{e}\mathrm{Re}\,c_R^{l_i l_i}, \quad \mathcal{B}(\mu \to e\gamma) = \frac{m_\mu^3}{4\pi\Gamma_\mu}(|c_R^{e\mu}|^2 + |c_R^{\mu e}|^2).$$

$$(10)$$

Note that there are in general no correlation between magnetic moments and lepton flavor violation [27]. When NP particles couple to muon and electron simultaneously, one expects $c_R^{e\mu} = \sqrt{c_R^{ee} c_R^{\mu\mu}}$ and the resulting $\mu \to e\gamma$ rate is

$$\mathcal{B}(\mu \to e\gamma) = \frac{\alpha m_\mu^2}{16 m_e \Gamma_\mu}|\Delta a_\mu \Delta a_e| \sim 8 \times 10^{-5}, \quad (11)$$

which excesses the MEG bound by 8 order of magnitude [27]. As an EFT approach only makes use of SM particles with all NP particles being integrated out, it is generic. For example, information on $\mathrm{Re}(c_R^{\mu\mu})$, $\mathrm{Re}(c_R^{ee})$ and $|c_R^{e\mu}|^2 + |c_R^{\mu e}|^2$ can be extracted from data without referring to any specific NP model. However, to correlate different quantities, such as $\Delta a_{\mu,e}$ and the $\mu \to e\gamma$ decay rate, one needs additional assumption on the underlying NP model. For example, the above $c_R^{e\mu} = \sqrt{c_R^{ee} c_R^{\mu\mu}}$ relation requires the NP particles to couple to muon and electron simultaneously [27]. The class of models adopted here provides a realization of this situation via one-loop diagrams in Fig. 1. In addition to the above discussion, note that the so-called F_1 photonic penguin and box contributions are usually lumped into the 4-lepton operators in an EFT approach. As a result, it will be difficult to separate them. The present approach is

(a) (b) (c) (d)
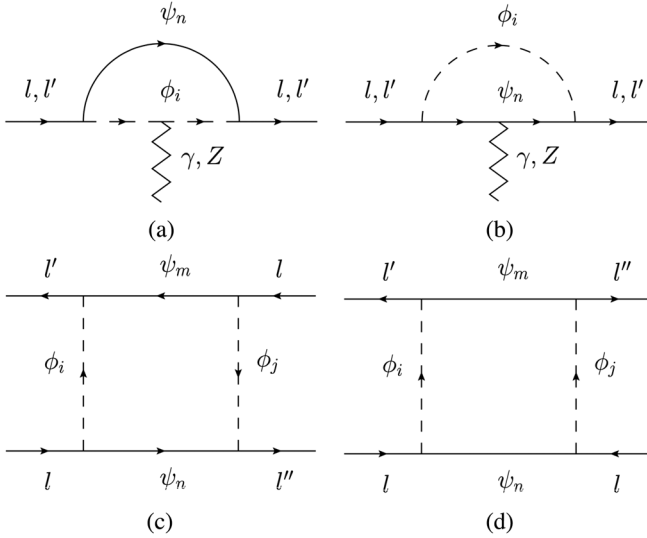
FIG. 1. Diagrams contributing to various processes. Penguin diagrams contributing to e, μ, and τ, $g-2$, d_l, $l' \to l\gamma$, $\bar{l}' \to l\bar{l}l$, and $l'N \to lN$ processes are shown in Figs. 1(a) and 1(b), while box diagrams contributing to the $\bar{l}' \to l\bar{l}''l$ process are shown in Figs. 1(c) and 1(d). Note that we do not show diagrams involving self energy parts. Figure 1(d) is for the Majorana case.

less generic than an EFT approach, but it is more generic than a specific model, as we try to capture some common behaviors or ingredients of a class of models concerning the lepton sector. It is in between of a specify model and an EFT approach and it can be a bridge to link them. When comparing to an EFT approach, the limitation of the present approach is its less of generality, while the advantage of it is the ability to provide some correlations and detail information, which are in general difficult to obtain in an EFT approach without introducing additional assumption.

In this work two cases are considered The first case does not have any built-in cancellation mechanism and the second case has some built-in mechanism, such as Glashow-Iliopoulos-Maiani or super-Glashow-Iliopoulos-Maiani mechanism. These two cases are complementary to each other and it will be interesting to compare them. This work is an updated and extended study of [82], where only μ decays were considered. Note that a similar setup, but in the quark sector, has been used in a study of the $b \to s\mu^+\mu^-$ decay [83].

We briefly give the framework in the next section. In Sec. III, numerical results will be presented, where data on $g-2$, d_l and upper limits of LFV rates will be used to constrain parameters and the correlations between different processes will be investigated. We give our conclusion in Sec. IV, which is followed by two Appendices.

II. FRAMEWORK

The generic interacting Lagrangian involving leptons (l), exotic spin-0 bosons (ϕ_i), and spin-1/2 fermions (ψ_n) is given by

$$\mathcal{L}_{\mathrm{int}} = \bar{\psi}_n(g_{lL}^{ni}P_L + g_{lR}^{ni}P_R)l\phi_i^* + \bar{l}(g_{lL}^{ni*}P_R + g_{lR}^{ni*}P_L)\psi_n\phi_i,$$

$$(12)$$

where indices, l, i and n, are summed and these fields are in their mass bases. It can contribute to lepton $g-2$, d_l and various LFV processes, such as $l' \to l\gamma$, $\bar{l}' \to l\bar{l}l$ decays and $l'N \to lN$ transitions, via diagrams shown in Fig. 1. Some useful formulas can be found in Ref. [82] and are collected in Appendix A.

As noted in the Introduction, we consider two complementary cases. In case I there is no any built-in cancellation mechanism. A typical amplitude, A, may contain several subamplitudes, A_j, each comes from one of the loop diagrams (see Fig. 1) giving

$$A = \sum_{j=1}^{N} A_j.$$

$$(13)$$

To constrain these subamplitudes from data, we will switch them on one at a time. Different subamplitudes are in principle independent from each other as there is no any built-in cancellation mechanism. However, in a realistic

TABLE II.   Terms contributing to various processes in case I.

Processes	γ-penguin	γ-penguin	Z-penguin	Box
Δa_l	$Q_{\phi,\psi}|g_{lL(R)}|^2$	$Q_{\phi,\psi}\mathrm{Re}(g_{lR}^*g_{lL})$		
d_l		$Q_{\phi,\psi}\mathrm{Im}(g_{lR}^*g_{lL})$		
$\mu^+ \to e^+\gamma$	$Q_{\phi,\psi}g_{\mu L(R)}^*g_{eL(R)}$	$Q_{\phi,\psi}g_{\mu R(L)}^*g_{eL(R)}$		
$\mu^+ \to e^-e^+e^-$	$Q_{\phi,\psi}g_{\mu L(R)}^*g_{eL(R)}$	$Q_{\phi,\psi}g_{\mu R(L)}^*g_{eL(R)}$	$g_{\mu R(L)}^*g_{eR(L)}\Delta T_{3\psi}(\kappa_{R(L)})$	$g_{\mu M}^*g_{eN}g_{eO}^*g_{eP}$
$\mu^-N \to e^-N$	$Q_{\phi,\psi}g_{\mu L(R)}g_{eL(R)}^*$	$Q_{\phi,\psi}g_{\mu R(L)}g_{eL(R)}^*$	$g_{\mu R(L)}g_{eR(L)}^*\Delta T_{3\psi}(\kappa_{R(L)})$	$g_{\mu M}g_{eN}^*g_{eO}g_{eP}^*$
$\tau^- \to e^-\gamma$	$Q_{\phi,\psi}g_{\tau L(R)}g_{eL(R)}^*$	$Q_{\phi,\psi}g_{\tau R(L)}g_{eL(R)}^*$		
$\tau^- \to e^-e^+e^-$	$Q_{\phi,\psi}g_{\tau L(R)}g_{eL(R)}^*$	$Q_{\phi,\psi}g_{\tau R(L)}g_{eL(R)}^*$	$g_{\tau R(L)}g_{eR(L)}^*\Delta T_{3\psi}(\kappa_{R(L)})$	$g_{\tau M}g_{eN}^*g_{eM}g_{eN}^*$
$\tau^- \to \mu^-\gamma$	$Q_{\phi,\psi}g_{\tau L(R)}g_{\mu L(R)}^*$	$Q_{\phi,\psi}g_{\tau R(L)}g_{\mu L(R)}^*$		
$\tau^- \to \mu^-\mu^+\mu^-$	$Q_{\phi,\psi}g_{\tau L(R)}g_{\mu L(R)}^*$	$Q_{\phi,\psi}g_{\tau R(L)}g_{\mu L(R)}^*$	$g_{\tau R(L)}g_{\mu R(L)}^*\Delta T_{3\psi}(\kappa_{R(L)})$	$g_{\tau M}g_{\mu N}^*g_{\mu M}g_{\mu N}^*$
$\tau^- \to e^-\mu^+e^-$				$g_{\tau M}g_{eN}^*g_{\mu M}g_{eN}^*$
$\tau^- \to \mu^-e^+\mu^+$				$g_{\tau M}g_{\mu N}^*g_{eM}g_{\mu N}^*$

model calculation, it is likely to have several amplitudes to appear at the same time and interfere. Nevertheless, it is well known that interference effects can be important only when the amplitudes are of similar size. For amplitudes of different sizes, this analysis can constrain the most dominant amplitude. On the other hand, through investigating the sizes of different subamplitudes the analysis can also identify the region, where several subamplitudes are of similar sizes, and, hence, identify where interference can be potentially important.

The Wilson coefficients of a typical subamplitude can be obtained by using formulas in Appendix A, but with the following replacement,

$$g_{lM}^{ni} \to g_{lM}. \tag{14}$$

Terms contributing to various processes in case I are shown in Table II. Note that $\Delta T_{3\psi}$ is basically the difference of weak isospin quantum numbers of ψ_R and ψ_L, while $\kappa_{R,L}$ are defined in Eq. (A12). Note that $\Delta T_{3\psi}$ is expected to be an order one quantity, while κ_R is expected to be a small quantity. See Appendix A for more information.
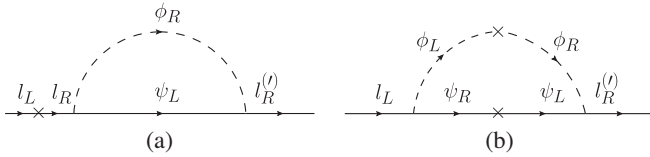
FIG. 2.   Two types of photonic dipole penguin diagrams (photon line not shown). The diagram in the left panel does not have the so-called chiral enhancement, while the one in the right panel has. The crosses denote mass insertions or mixings that connect l_L and l_R, ψ_L and ψ_R, ϕ_L and ϕ_R fields. Since l_L and l_R have different weak quantum numbers, the cross in the left diagram and one of the crosses in the right diagram need to couple to the Higgs VEV, while the other cross in the right diagram connects fields with identical weak quantum numbers. See text for more details.

In Fig. 2 we gives two typical diagrams contributing to the photonic dipole penguins. The left diagram can occur in a chiral interaction, while the right diagram is possible only for the so-called nonchiral interaction, where ϕ and ψ couple to both l_L and $l_R^{(\prime)}$ at the same time. It is well known in the literature, see, for example, Ref. [84], that a nonchiral interaction can provide chiral enhancement in photonic dipole penguin amplitudes resulting in sizable effects in quantities and processes such as Δa_l, $l \to l'\gamma$ decays and so on. A way to see this is by using the EFT approach. Before spontaneous symmetry breaking, we have the following dipole operators, [80]

$$Q_{eW} = (\bar{L}_L\sigma^{\mu\nu}l_R)\tau^I HW_{\mu\nu}^I, \qquad Q_{eB} = (\bar{L}_L\sigma^{\mu\nu}l_R)HB_{\mu\nu}, \tag{15}$$

where L_L, l_R are the isodoublet and singlet lepton fields, $W_{\mu\nu}$ and $B_{\mu\nu}$ are the $SU(2)$ and $U(1)$ field strengths, and H is the Higgs field. To obtain a photonic dipole interaction term as shown in Eq. (9), one needs the above operators, but with the Higgs field replaced by its vacuum expectation value (VEV), i.e., $H \to \langle H \rangle$. In Fig. 2(a), the Higgs-lepton-lepton Yukawa vertex applies to the external lepton line with the Higgs field replaced by its VEV, while in Fig. 2(b), it is required to have either ψ_L and ψ_R or ϕ_L and ϕ_R being mixed due to a Higgs VEV, and the other pair of fields with identical quantum numbers. It is clear that the left and right diagrams in Fig. 2 are associated with m_l and m_ψ, respectively, and the mass ratio gives rise to the chiral enhancement. It is important to note that only fields with suitable weak quantum numbers that mix due to a Higgs VEV can have nonchiral interaction generating chiral enhancement. Hence, it is nontrivial to have chiral enhancement in a new physics model. For the possible $SU(2) \times U(1)$ quantum numbers of ψ and ϕ, and the combinations that can generate the nonchiral interaction resulting chiral enhancement, see Appendix B.

TABLE III.   Terms contributing to various processes in case II.

Processes	γ-penguin	γ-penguin	Z-penguin	Box
Δa_l	$Q_{\phi,\psi}|g_{lL(R)}|^2$	$Q_{\phi,\psi}\text{Re}(g_{lR}^*g_{lL}\delta_{RL}^{ll})$		
d_l		$Q_{\phi,\psi}\text{Im}(g_{lR}^*g_{lL}\delta_{RL}^{ll})$		
$\mu^+ \to e^+\gamma$	$Q_{\phi,\psi}g_{\mu M}^*g_{eM}\delta_{MM}^{\mu e}$	$Q_{\phi,\psi}g_{\mu R(L)}^*g_{eL(R)}\delta_{RL(LR)}^{\mu e}$		
$\mu^+ \to e^-e^+e^-$	$Q_{\phi,\psi}g_{\mu M}^*g_{eM}\delta_{MM}^{\mu e}$	$Q_{\phi,\psi}g_{\mu R(L)}^*g_{eL(R)}\delta_{RL(LR)}^{\mu e}$	$g_{\mu M}^*g_{eM}\Delta T_{3\psi}\delta_{MM}^{\mu e}$	$g_{\mu M}^*g_{eM}g_{eN}^*g_{eN}\delta_{MM}^{\mu e}$
$\mu^-N \to e^-N$	$Q_{\phi,\psi}g_{\mu M}g_{eM}^*\delta_{MM}^{e\mu}$	$Q_{\phi,\psi}g_{\mu R(L)}g_{eL(R)}^*\delta_{LR(RL)}^{e\mu}$	$g_{\mu M}g_{eM}^*\Delta T_{3\psi}\delta_{MM}^{e\mu}$	$g_{\mu M}g_{eM}^*g_{eN}g_{eN}^*\delta_{MM}^{e\mu}$
$\tau^- \to e^-\gamma$	$Q_{\phi,\psi}g_{\tau M}g_{eM}^*\delta_{MM}^{e\tau}$	$Q_{\phi,\psi}g_{\tau R(L)}g_{eL(R)}^*\delta_{LR(RL)}^{e\tau}$		
$\tau^- \to e^-e^+e^-$	$Q_{\phi,\psi}g_{\tau M}g_{eM}^*\delta_{MM}^{e\tau}$	$Q_{\phi,\psi}g_{\tau R(L)}g_{eL(R)}^*\delta_{LR(RL)}^{e\tau}$	$g_{\tau M}g_{eM}^*\Delta T_{3\psi}\delta_{MM}^{e\tau}$	$g_{\tau M}g_{eM}^*g_{eN}g_{eN}^*\delta_{MM}^{e\tau}$
$\tau^- \to \mu^-\gamma$	$Q_{\phi,\psi}g_{\tau M}g_{\mu M}^*\delta_{MM}^{e\tau}$	$Q_{\phi,\psi}g_{\tau R(L)}g_{\mu L(R)}^*\delta_{LR(RL)}^{e\tau}$		
$\tau^- \to \mu^-\mu^+\mu^-$	$Q_{\phi,\psi}g_{\tau M}g_{\mu M}^*\delta_{MM}^{\mu\tau}$	$Q_{\phi,\psi}g_{\tau R(L)}g_{\mu L(R)}^*\delta_{LR(RL)}^{\mu\tau}$	$g_{\tau M}g_{\mu M}^*\Delta T_{3\psi}\delta_{MM}^{\mu\tau}$	$g_{\tau M}g_{\mu M}^*g_{\mu N}g_{\mu N}^*\delta_{MM}^{\mu\tau}$
$\tau^- \to e^-\mu^+e^-$				$g_{\tau M}g_{eN}^*g_{\mu O}g_{eP}^*\delta_{NM}^{e\tau}\delta_{PO}^{e\mu}$
$\tau^- \to \mu^-e^+\mu^+$				$g_{\tau M}g_{\mu M}^*g_{eO}g_{\mu P}^*\delta_{NM}^{\mu\tau}\delta_{PO}^{\mu e}$

In the second case (case II), there is a built-in cancellation mechanism. Now some subamplitudes in Eq. (13) are related intimately. They need to be grouped together to allow the cancellation mechanism to take place, and the resulting group of amplitudes should be viewed as a new subamplitude. To constrain these new subamplitudes from data, we will turn them on one at a time. To be specify, we consider the following replacement,

$$g_{lM}^{ni} \to g_{lM}^i = g_{lM}\Gamma_M^{il}, \qquad (16)$$

where g_{lM} is real (as the phase is absorbed into Γ_M) and we have $M = L, R$. These Γ satisfy the following relations:

$$\Gamma_M^{\dagger li}m_i^2\Gamma_N^{il'} = (m_\phi^2)_{MN}^{ll'}, \qquad \Gamma_M^{\dagger li}\Gamma_N^{il'} = \delta^{ll'}\delta_{MN}, \quad (17)$$

where the δs are Kronecker deltas. Typical terms in a Wilson coefficient given in Appendix A should now be replaced accordingly:

$$\sum_i g_{l'M}^{i*}f(m_\psi^2,m_{\phi_i}^2)g_{lN}^i \to m_\phi^2\frac{\partial}{\partial m_\phi^2}f(m_\psi^2,m_\phi^2)g_{\mu M}g_{eN}\delta_{l'l}^{MN}, \qquad (18)$$

where m_ϕ^2 is the average of the mass squared of ϕ_i and $\delta_{l'l}^{MN}$ is the mixing angle defined in the usual way (do not confuse it with the Kronecker delta): [84]

$$\delta_{l'l}^{MN} \equiv \frac{1}{m_\phi^2}\Gamma_{l'i}^{M\dagger}(m_{\phi_i}^2 - m_\phi^2)\Gamma_{il}^N = \frac{(m_\phi^2)_{l'l}^{MN}}{m_\phi^2}. \quad (19)$$

Note that as a common practice only the leading terms of δ are kept in the amplitudes. Therefore, to employ the "δ" parametrization, one needs to assume a large degree of flavor-alignment of the new fields to the SM leptons, i.e., the mass matrices of these new fields are almost diagonal in the mass basis of the SM leptons, and the small misalignment can be encoded in these δs. Usually this requires introducing additional symmetry to the model.

Terms contributing to various processes in case II are shown in Table III.

III. RESULTS

In this section we present the numerical results for cases I and II. Experimental inputs are from Refs. [4,17,18,22–24] and are shown in Table I. Further inputs not listed in the table are from Ref. [4].

A. Case I

In Table IV, we present the constraints on parameters in case I using $x \equiv m_\phi/m_\psi = 1$ and $m_\psi = 500$ GeV. Results for other m_ψ can be obtained by scaling the results with a $\frac{m_\psi}{500\text{ GeV}}$ factor for $Q_{\phi,\psi}g_{l^{(\prime)}R}^*g_{lL}$ and $(\frac{m_\psi}{500\text{ GeV}})^2$ for other quantities. Results in […] are obtained by using the future experimental sensitivities. Both results for the cases of Dirac and Majorana fermion are given, where results in {…} are for the Majorana case. Note that some of the results are unphysical. For example, the values of $Q_{\phi,\psi}|g_{eR}|^2$ and $Q_{\phi,\psi}|g_{\mu R}|^2$ required to produce large enough Δa_e and Δa_μ as required by data are much larger than 4π. Perturbative calculation breaks down and the results are untrustworthy, hence, unphysical. We naïvely state these results simply to indicate that contributions from $Q_{\phi,\psi}|g_{eR}|^2$ and $Q_{\phi,\psi}|g_{\mu R}|^2$ cannot generate the desired results on Δa_e and Δa_μ. Results for $x = 0.5$ and 2 are given in Tables V and VI, respectively.

In Figs. 3(a) and 3(b), we show the allowed parameter space for $\mp Q_{\phi,\psi}|g_{eL(R)}|^2$, $\mp Q_{\phi,\psi}\text{Re}(g_{eR}^*g_{eL})$, and $|Q_{\phi,\psi}\text{Im}(g_{eR}^*g_{eL})|$ constrained by Δa_e and d_e. In Figs. 3(c) and 3(d), allowed parameter space for $\pm Q_{\phi,\psi}|g_{\mu L(R)}|^2$, $\pm Q_{\phi,\psi}\text{Re}(g_{\mu R}^*g_{\mu L})$, and $|Q_{\phi,\psi}\text{Im}(g_{\mu R}^*g_{\mu L})|$ constrained by Δa_μ and d_μ are shown. In Fig. 3(e) the allowed parameter

TABLE IV. Constraints on parameters in case I using $x \equiv m_\phi/m_\psi = 1$ and $m_\psi = 500$ GeV from various processes are shown. Results are applicable with L and R interchanged. Results for other m_ψ can be obtained by scaling with a $(\frac{m_\psi}{500\,\text{GeV}})^2$ or $\frac{m_\psi}{500\,\text{GeV}}$ factor, where the latter is for $Q_{\phi,\psi} g^*_{l^{(\prime)}R} g_{lL}$. Results in [...] are obtained by using the future experimental sensitivities, results in {...} are for the Majorana case.

Processes	Constraints	Constraints	Constraints	Constraints
	$Q_\phi \lvert g_{eR}\rvert^2$	$Q_\psi \lvert g_{eR}\rvert^2$	$Q_\phi \mathrm{Re}(g^*_{eR} g_{eL})$	$Q_\psi \mathrm{Re}(g^*_{eR} g_{eL})$
Δa_e	-1597 ± 653	1597 ∓ 653	$(-4.1 \pm 1.6) \times 10^{-4}$	$(2.0 \mp 0.8) \times 10^{-4}$
	$Q_\phi \lvert g_{\mu R}\rvert^2$	$Q_\psi \lvert g_{\mu R}\rvert^2$	$Q_\phi \mathrm{Re}(g^*_{\mu R} g_{\mu L})$	$Q_\psi \mathrm{Re}(g^*_{\mu R} g_{\mu L})$
Δa_μ	115 ± 31	-115 ∓ 31	$(6.1 \pm 1.6) \times 10^{-3}$	$(-3.0 \mp 0.8) \times 10^{-3}$
	$Q_\phi \lvert g_{\tau R}\rvert^2$	$Q_\psi \lvert g_{\tau R}\rvert^2$	$Q_\phi \mathrm{Re}(g^*_{\tau R} g_{\tau L})$	$Q_\psi \mathrm{Re}(g^*_{\tau R} g_{\tau L})$
Δa_τ	$(-7 \sim 2) \times 10^6$	$(-2 \sim 7) \times 10^6$	$(-7 \sim 2) \times 10^3$	$(-0.8 \sim 3) \times 10^3$
	$\lvert Q_\phi \mathrm{Im}(g^*_{eR} g_{eL})\rvert$	$\lvert Q_\phi \mathrm{Im}(g^*_{eR} g_{eL})\rvert$	$\lvert Q_\phi \mathrm{Im}(g^*_{\mu(\tau)R} g_{\mu(\tau)L})\rvert$	$\lvert Q_\psi \mathrm{Im}(g^*_{\mu(\tau)R} g_{\mu(\tau)L})\rvert$
$d_e,\ d_\mu,\ d_\tau$	2.6×10^{-10}	1.3×10^{-10}	$4.6(38.3)$	$2.3(19.1)$
	$\lvert Q_\phi g^*_{\mu R} g_{eR}\rvert$	$\lvert Q_\psi g^*_{\mu R} g_{eR}\rvert$	$\lvert Q_\phi g^*_{\mu R} g_{eL}\rvert$	$\lvert Q_\psi g^*_{\mu R} g_{eL}\rvert$
$\mu^+ \to e^+\gamma$	$0.002[0.0008]$	$0.002[0.0008]$	$11[4] \times 10^{-8}$	$6[2] \times 10^{-8}$
$\mu^+ \to e^-e^+e^-$	$0.046[0.0005]$	$0.030[0.0003]$	$224[2] \times 10^{-8}$	$112[1] \times 10^{-8}$
$\mu^- \mathrm{Au} \to e^-\mathrm{Au}$	$0.020[0.0002]$	$0.016[0.0002]$	$236[3] \times 10^{-8}$	$118[1] \times 10^{-8}$
$\mu^- \mathrm{Ti} \to e^-\mathrm{Ti}$	$0.051[0.00008]$	$0.046[0.00007]$	$569[0.9] \times 10^{-8}$	$284[0.4] \times 10^{-8}$
$\mu^- \mathrm{Al} \to e^-\mathrm{Al}$	$[0.00010]$	$[0.00009]$	$[1.1 \times 10^{-8}]$	$[0.5 \times 10^{-8}]$
	$\lvert g^*_{\mu R} g_{eR} \Delta T_{3\psi}\rvert$	$\lvert g^*_{\mu R} g_{eR} \kappa_R\rvert$	$\lvert g^*_{\mu R} g_{eR} g^*_{eR} g_{eR}\rvert$	$\lvert g^*_{\mu R} g_{eR} g^*_{eL} g_{eL}\rvert$
$\mu^+ \to e^-e^+e^-$	$393[4] \times 10^{-6}$	$115[1] \times 10^{-6}$	$0.01\{-\}[1 \times 10^{-4}\{-\}]$	$7\{7\} \times 10^{-3}[7\{7\} \times 10^{-5}]$
$\mu^- \mathrm{Au} \to e^-\mathrm{Au}$	$492[6] \times 10^{-7}$	$145[2] \times 10^{-7}$		
$\mu^- \mathrm{Ti} \to e^-\mathrm{Ti}$	$1718[3] \times 10^{-7}$	$5049[8] \times 10^{-8}$		
$\mu^- \mathrm{Al} \to e^-\mathrm{Al}$	$[4 \times 10^{-7}]$	$[1 \times 10^{-7}]$		
	$\lvert Q_\phi g_{\tau R} g^*_{eR}\rvert$	$\lvert Q_\psi g_{\tau R} g^*_{eR}\rvert$	$\lvert Q_\phi g_{\tau R} g^*_{eL}\rvert$	$\lvert Q_\psi g_{\tau R} g^*_{eL}\rvert$
$\tau^- \to e^-\gamma$	$1.4[0.4]$	$1.4[0.4]$	$13[4] \times 10^{-4}$	$6[2] \times 10^{-4}$
$\tau^- \to e^-e^+e^-$	$13.2[1.7]$	$10.0[1.3]$	$11[1] \times 10^{-3}$	$56[7] \times 10^{-4}$
	$\lvert g_{\tau R} g^*_{eR} \Delta T_{3\psi}\rvert$	$\lvert g_{\tau R} g^*_{eR} \kappa_R\rvert$	$\lvert g_{\tau R} g^*_{eR} g_{eR} g^*_{eR}\rvert$	$\lvert g_{\tau R} g^*_{eR} g_{eL} g^*_{eL}\rvert$
$\tau^- \to e^-e^+e^-$	$0.15[0.02]$	$0.05[0.006]$	$4.3\{-\}[0.5\{-\}]$	$2.9\{2.9\}[0.4\{0.4\}]$
	$\lvert Q_\phi g_{\tau R} g^*_{\mu R}\rvert$	$\lvert Q_\psi g_{\tau R} g^*_{\mu R}\rvert$	$\lvert Q_\phi g_{\tau R} g^*_{\mu L}\rvert$	$\lvert Q_\psi g_{\tau R} g^*_{\mu L}\rvert$
$\tau^- \to \mu^-\gamma$	$1.7[0.3]$	$1.7[0.3]$	$15[2] \times 10^{-4}$	$7[1] \times 10^{-4}$
$\tau^- \to \mu^-\mu^+\mu^-$	$30.7[3.9]$	$12.5[1.6]$	$21[3] \times 10^{-3}$	$11[1] \times 10^{-3}$
	$\lvert g_{\tau R} g^*_{\mu R} \Delta T_{3\psi}\rvert$	$\lvert g_{\tau R} g^*_{\mu R} \kappa_R\rvert$	$\lvert g_{\tau R} g^*_{\mu R} g_{\mu R} g^*_{\mu R}\rvert$	$\lvert g_{\tau R} g^*_{\mu R} g_{\mu L} g^*_{\mu L}\rvert$
$\tau^- \to \mu^-\mu^+\mu^-$	$0.14[0.02]$	$0.04[0.005]$	$3.8\{-\}[0.5\{-\}]$	$2.5\{2.5\}[0.3\{0.3\}]$
	$\lvert g_{\tau R} g^*_{eR} g_{\mu R} g^*_{eR}\rvert$	$\lvert g_{\tau R} g^*_{eR} g_{\mu L} g^*_{eL}\rvert$	$\lvert g_{\tau R} g^*_{eL} g_{\mu R} g^*_{eL}\rvert$	
$\tau^- \to e^-\mu^+e^-$	$3.2\{-\}[0.4\{-\}]$	$2.3\{2.3\}[0.3\{0.3\}]$	$6.4\{6.4\}[0.8\{0.8\}]$	
	$\lvert g_{\tau R} g^*_{\mu R} g_{eR} g^*_{\mu R}\rvert$	$\lvert g_{\tau R} g^*_{\mu R} g_{eL} g^*_{\mu L}\rvert$	$\lvert g_{\tau R} g^*_{\mu L} g_{eR} g^*_{\mu L}\rvert$	
$\tau^- \to \mu^-e^+\mu^+$	$3.4\{-\}[0.4\{-\}]$	$2.4\{2.4\}[0.3\{0.3\}]$	$6.8\{6.8\}[0.9\{0.9\}]$	

space for $\lvert Q_{\phi,\psi} g^*_{\mu R(L)} g_{eL(R)}\rvert$ constrained by $\mu \to e\gamma$ and the parameter space on $\lvert Q_{\phi,\psi}\rvert \lvert \mathrm{Re}(g^*_{eR} g_{eL}) \mathrm{Re}(g^*_{\mu R} g_{\mu L})\rvert^{1/2}$ to produce Δa_e and Δa_μ are presented. These results are given for $m_\psi = 500$ GeV. For other m_ψ, scale plots in (a) and (c) with $(500\,\text{GeV}/m_\psi)^2$, and scale plots in (b), (d) and (e) with $500\,\text{GeV}/m_\psi$.

In Figs. 4–6, the parameter space excluded or projected by various bounds or expected sensitivities on $\mu \to e$, $\tau \to e$, and $\tau \to \mu$ lepton flavor violating processes

are shown. They are contributed from photonic penguin, Z-penguin and box diagrams. In Fig. 7, the parameter space excluded or projected by using various bounds or projected sensitivities on $\tau^- \to e^-\mu^+e^-, \mu^-e^+\mu^-$ processes through contributions from box diagrams are shown.

From these results we can extract several messages. First we note that chiral interactions ($g_L \times g_R = 0$) are unable to generate large enough Δa_e and Δa_μ to accommodate the experimental results, Eqs. (1) and (2). From Tables IV–VI,

TABLE V. Same as Table IV, but with $x \equiv m_\phi/m_\psi = 0.5$.

Processes	Constraints	Constraints	Constraints	Constraints
	$Q_\phi|g_{eR}|^2$	$Q_\psi|g_{eR}|^2$	$Q_\phi\mathrm{Re}(g_{eR}^*g_{eL})$	$Q_\psi\mathrm{Re}(g_{eR}^*g_{eL})$
Δa_e	-811 ± 332	1059 ∓ 433	$(-2.3 \pm 1.0) \times 10^{-4}$	$(1.5 \mp 0.7) \times 10^{-4}$
	$Q_\phi|g_{\mu R}|^2$	$Q_\psi|g_{\mu R}|^2$	$Q_\phi\mathrm{Re}(g_{\mu R}^*g_{\mu L})$	$Q_\psi\mathrm{Re}(g_{\mu R}^*g_{\mu L})$
Δa_μ	58 ± 16	-76 ∓ 20	$(3.5 \pm 0.9) \times 10^{-3}$	$(-2.3 \mp 0.6) \times 10^{-3}$
	$Q_\phi|g_{\tau R}|^2$	$Q_\psi|g_{\tau R}|^2$	$Q_\phi\mathrm{Re}(g_{\tau R}^*g_{\tau L})$	$Q_\psi\mathrm{Re}(g_{\tau R}^*g_{\tau L})$
Δa_τ	$(-4 \sim 1) \times 10^6$	$(-1 \sim 5) \times 10^6$	$(-4 \sim 1) \times 10^3$	$(-0.7 \sim 3) \times 10^3$
	$|Q_\phi\mathrm{Im}(g_{eR}^*g_{eL})|$	$|Q_\phi\mathrm{Im}(g_{eR}^*g_{eL})|$	$|Q_\phi\mathrm{Im}(g_{\mu(\tau)R}^*g_{\mu(\tau)L})|$	$|Q_\psi\mathrm{Im}(g_{\mu(\tau)R}^*g_{\mu(\tau)L})|$
d_e, d_μ, d_τ	1.5×10^{-10}	1.0×10^{-10}	$2.6(22.0)$	$1.8(14.9)$
	$|Q_\phi g_{\mu R}^*g_{eR}|$	$|Q_\psi g_{\mu R}^*g_{eR}|$	$|Q_\phi g_{\mu R}^*g_{eL}|$	$|Q_\psi g_{\mu R}^*g_{eL}|$
$\mu^+ \to e^+\gamma$	$0.001[0.0004]$	$0.001[0.0005]$	$7[2] \times 10^{-8}$	$4[2] \times 10^{-8}$
$\mu^+ \to e^-e^+e^-$	$0.024[0.0002]$	$0.021[0.0002]$	$129[1] \times 10^{-8}$	$87[0.9] \times 10^{-8}$
$\mu^-\mathrm{Au} \to e^-\mathrm{Au}$	$0.008[0.0001]$	$0.013[0.0002]$	$136[2] \times 10^{-8}$	$92[1] \times 10^{-8}$
$\mu^-\mathrm{Ti} \to e^-\mathrm{Ti}$	$0.022[0.00003]$	$0.038[0.00006]$	$327[0.5] \times 10^{-8}$	$222[0.3] \times 10^{-8}$
$\mu^-\mathrm{Al} \to e^-\mathrm{Al}$	$[4 \times 10^{-5}]$	$[7 \times 10^{-5}]$	$[6.2 \times 10^{-9}]$	$[4.2 \times 10^{-9}]$
	$|g_{\mu R}^*g_{eR}\Delta T_{3\psi}|$	$|g_{\mu R}^*g_{eR}\kappa_R|$	$|g_{\mu R}^*g_{eR}g_{eR}^*g_{eR}|$	$|g_{\mu R}^*g_{eR}g_{eL}^*g_{eL}|$
$\mu^+ \to e^-e^+e^-$	$274[3] \times 10^{-6}$	$148[1] \times 10^{-6}$	$6\{7\} \times 10^{-3}[6\{7\} \times 10^{-5}]$	$3\{3\} \times 10^{-3}[3\{3\} \times 10^{-5}]$
$\mu^-\mathrm{Au} \to e^-\mathrm{Au}$	$343[4] \times 10^{-7}$	$186[2] \times 10^{-7}$		
$\mu^-\mathrm{Ti} \to e^-\mathrm{Ti}$	$1120[2] \times 10^{-7}$	$649[1] \times 10^{-7}$		
$\mu^-\mathrm{Al} \to e^-\mathrm{Al}$	$[3 \times 10^{-7}]$	$[1 \times 10^{-7}]$		
	$|Q_\phi g_{\tau R}g_{eR}^*|$	$|Q_\psi g_{\tau R}g_{eR}^*|$	$|Q_\phi g_{\tau R}g_{eL}^*|$	$|Q_\psi g_{\tau R}g_{eL}^*|$
$\tau^- \to e^-\gamma$	$0.7[0.2]$	$1.0[0.3]$	$7[2] \times 10^{-4}$	$5[1] \times 10^{-4}$
$\tau^- \to e^-e^+e^-$	$6.8[0.9]$	$6.9[0.9]$	$65[8] \times 10^{-4}$	$44[6] \times 10^{-4}$
	$|g_{\tau R}g_{eR}^*\Delta T_{3\psi}|$	$|g_{\tau R}g_{eR}^*\kappa_R|$	$|g_{\tau R}g_{eR}^*g_{eR}g_{eR}^*|$	$|g_{\tau R}g_{eR}^*g_{eL}g_{eL}^*|$
$\tau^- \to e^-e^+e^-$	$0.11[0.01]$	$0.06[0.007]$	$2.5\{2.7\}[0.3\{0.3\}]$	$1.1\{1.1\}[0.1\{0.1\}]$
	$|Q_\phi g_{\tau R}g_{\mu R}^*|$	$|Q_\psi g_{\tau R}g_{\mu R}^*|$	$|Q_\phi g_{\tau R}g_{\mu L}^*|$	$|Q_\psi g_{\tau R}g_{\mu L}^*|$
$\tau^- \to \mu^-\gamma$	$0.8[0.1]$	$1.1[0.2]$	$9[1] \times 10^{-4}$	$58[9] \times 10^{-5}$
$\tau^- \to \mu^-\mu^+\mu^-$	$16.7[2.1]$	$8.9[1.1]$	$12[2] \times 10^{-3}$	$8[1] \times 10^{-3}$
	$|g_{\tau R}g_{\mu R}^*\Delta T_{3\psi}|$	$|g_{\tau R}g_{\mu R}^*\kappa_R|$	$|g_{\tau R}g_{\mu R}^*g_{\mu R}g_{\mu R}^*|$	$|g_{\tau R}g_{\mu R}^*g_{\mu L}g_{\mu L}^*|$
$\tau^- \to \mu^-\mu^+\mu^-$	$0.09[0.01]$	$0.05[0.006]$	$2.2\{2.4\}[0.3\{0.3\}]$	$1.0\{1.0\}[0.1\{0.1\}]$
	$|g_{\tau R}g_{eR}^*g_{\mu R}g_{eR}^*|$	$|g_{\tau R}g_{eR}^*g_{\mu L}g_{eL}^*|$	$|g_{\tau R}g_{eL}^*g_{\mu R}g_{eL}^*|$	
$\tau^- \to e^-\mu^+e^-$	$1.8\{2.0\}[0.2\{0.3\}]$	$0.9\{0.9\}[0.1\{0.1\}]$	$1.9\{1.9\}[0.2\{0.2\}]$	
	$|g_{\tau R}g_{\mu R}^*g_{eR}g_{\mu R}^*|$	$|g_{\tau R}g_{\mu R}^*g_{eL}g_{\mu L}^*|$	$|g_{\tau R}g_{\mu L}^*g_{eR}g_{\mu L}^*|$	
$\tau^- \to \mu^-e^+\mu^+$	$2.0\{2.2\}[0.2\{0.3\}]$	$1.0\{1.0\}[0.1\{0.1\}]$	$2.1\{2.1\}[0.3\{0.3\}]$	

Figs. 3(a) and 3(c), we see that $Q_{\phi,\psi}|g_{eR(L)}|^2$ and $Q_{\phi,\psi}|g_{\mu R(L)}|^2$ need to be unreasonably large to produce the experimental value of Δa_e and Δa_μ. This implies the incapability of chiral interactions to generate large enough Δa_e and Δa_μ to accommodate the experimental results.

Although nonchiral interactions are capable to generate Δa_e and Δa_μ successfully accommodating the experimental results, they are not contributed from the same source. From Tables IV–VI, we see that, for $x = 0.5$, 1, and 2, $Q_{\phi,\psi}\mathrm{Re}(g_{eR}^*g_{eL})$ and $Q_{\phi,\psi}\mathrm{Re}(g_{\mu R}^*g_{\mu L})$ of orders 10^{-4} and 10^{-3}, respectively, are able to produce the experimental values of Δa_e and Δa_μ. However, the contributions cannot come from the same source, i.e., from diagrams involving the same set of ϕ and ψ. The reasons are as follows. If Δa_e and Δa_μ are generated from the same set of ψ and ϕ, the very same set of ψ and ϕ will also generate $\mu \to e\gamma$ decay with rate exceeding the experimental bound. Indeed, from Fig. 3(e) we see that the $\mu \to e\gamma$ data constraints $|Q_{\phi,\psi}g_{\mu R(L)}^*g_{eL(R)}|$ to be less than 10^{-7} to 10^{-6}, but experimental data on Δa_e and Δa_μ require $|Q_{\phi,\psi}||\mathrm{Re}(g_{eR}^*g_{eL})\mathrm{Re}(g_{\mu R}^*g_{\mu L})|^{1/2}$ to be of the order of 10^{-3} to 10^{-1}, which is larger than the constrain from $\mu \to e\gamma$ by more than 4 orders of magnitude. Hence, the contributions to Δa_e and Δa_μ do not come from the same

TABLE VI. Same as Table IV, but with $x \equiv m_\phi/m_\psi = 2$.

Processes	Constraints	Constraints	Constraints	Constraints
	$Q_\phi|g_{eR}|^2$	$Q_\psi|g_{eR}|^2$	$Q_\phi\text{Re}(g_{eR}^* g_{eL})$	$Q_\psi\text{Re}(g_{eR}^* g_{eL})$
Δa_e	-4234 ± 1732	3247 ∓ 1328	$(-9.4 \pm 3.8) \times 10^{-4}$	$(3.2 \mp 1.3) \times 10^{-4}$
	$Q_\phi|g_{\mu R}|^2$	$Q_\psi|g_{\mu R}|^2$	$Q_\phi\text{Re}(g_{\mu R}^* g_{\mu L})$	$Q_\psi\text{Re}(g_{\mu R}^* g_{\mu L})$
Δa_μ	305 ± 82	-234 ∓ 63	$(14.0 \pm 3.7) \times 10^{-3}$	$(-4.8 \mp 1.3) \times 10^{-3}$
	$Q_\phi|g_{\tau R}|^2$	$Q_\psi|g_{\tau R}|^2$	$Q_\phi\text{Re}(g_{\tau R}^* g_{\tau L})$	$Q_\psi\text{Re}(g_{\tau R}^* g_{\tau L})$
Δa_τ	$(-20 \sim 5) \times 10^6$	$(-4 \sim 16) \times 10^6$	$(-16 \sim 4) \times 10^3$	$(-1 \sim 5) \times 10^3$
	$|Q_\phi\text{Im}(g_{eR}^* g_{eL})|$	$|Q_\phi\text{Im}(g_{eR}^* g_{eL})|$	$|Q_\phi\text{Im}(g_{\mu(\tau)R}^* g_{\mu(\tau)L})|$	$|Q_\psi\text{Im}(g_{\mu(\tau)R}^* g_{\mu(\tau)L})|$
d_e, d_μ, d_τ	6.1×10^{-10}	2.1×10^{-10}	$10.5(88.1)$	$3.6(30.3)$
	$|Q_\phi g_{\mu R}^* g_{eR}|$	$|Q_\psi g_{\mu R}^* g_{eR}|$	$|Q_\phi g_{\mu R}^* g_{eL}|$	$|Q_\psi g_{\mu R}^* g_{eL}|$
$\mu^+ \to e^+\gamma$	$0.006[0.002]$	$0.004[0.002]$	$26[10] \times 10^{-8}$	$9[3] \times 10^{-8}$
$\mu^+ \to e^-e^+e^-$	$0.120[0.001]$	$0.056[0.0006]$	$516[5] \times 10^{-8}$	$177[2] \times 10^{-8}$
$\mu^-\text{Au} \to e^-\text{Au}$	$0.059[0.0007]$	$0.024[0.0003]$	$542[6] \times 10^{-8}$	$187[2] \times 10^{-8}$
$\mu^-\text{Ti} \to e^-\text{Ti}$	$0.151[0.0002]$	$0.069[0.0001]$	$1309[2] \times 10^{-8}$	$450[0.7] \times 10^{-8}$
$\mu^-\text{Al} \to e^-\text{Al}$	$[0.0003]$	$[0.0001]$	$[2.5 \times 10^{-8}]$	$[0.9 \times 10^{-8}]$
	$|g_{\mu R}^* g_{eR}\Delta T_{3\psi}|$	$|g_{\mu R}^* g_{eR}\kappa_R|$	$|g_{\mu R}^* g_{eR}g_{eR}^* g_{eR}|$	$|g_{\mu R}^* g_{eR}g_{eL}^* g_{eL}|$
$\mu^+ \to e^-e^+e^-$	$695[7] \times 10^{-6}$	$879[9] \times 10^{-7}$	$0.03\{0.05\}[2\{5\} \times 10^{-4}]$	$0.02\{0.02\}[2\{2\} \times 10^{-4}]$
$\mu^-\text{Au} \to e^-\text{Au}$	$87[1] \times 10^{-6}$	$110[1] \times 10^{-7}$		
$\mu^-\text{Ti} \to e^-\text{Ti}$	$3038[5] \times 10^{-7}$	$3845[6] \times 10^{-8}$		
$\mu^-\text{Al} \to e^-\text{Al}$	$[7 \times 10^{-7}]$	$[8 \times 10^{-8}]$		
	$|Q_\phi g_{\tau R}g_{eR}^*|$	$|Q_\psi g_{\tau R}g_{eR}^*|$	$|Q_\phi g_{\tau R}g_{eL}^*|$	$|Q_\psi g_{\tau R}g_{eL}^*|$
$\tau^- \to e^-\gamma$	$3.8[1.1]$	$2.9[0.9]$	$29[8] \times 10^{-4}$	$10[3] \times 10^{-4}$
$\tau^- \to e^-e^+e^-$	$34.7[4.4]$	$19.1[2.4]$	$26[3] \times 10^{-3}$	$9[1] \times 10^{-3}$
	$|g_{\tau R}g_{eR}^*\Delta T_{3\psi}|$	$|g_{\tau R}g_{eR}^*\kappa_R|$	$|g_{\tau R}g_{eR}^*g_{eR}g_{eR}^*|$	$|g_{\tau R}g_{eR}^*g_{eL}g_{eL}^*|$
$\tau^- \to e^-e^+e^-$	$0.27[0.03]$	$0.03[0.004]$	$9.9\{18.9\}[1.2\{2.4\}]$	$9.2\{9.2\}[1.2\{1.2\}]$
	$|Q_\phi g_{\tau R}g_{\mu R}^*|$	$|Q_\psi g_{\tau R}g_{\mu R}^*|$	$|Q_\phi g_{\tau R}g_{\mu L}^*|$	$|Q_\psi g_{\tau R}g_{\mu L}^*|$
$\tau^- \to \mu^-\gamma$	$4.4[0.7]$	$3.4[0.5]$	$34[5] \times 10^{-4}$	$11[2] \times 10^{-4}$
$\tau^- \to \mu^-\mu^+\mu^-$	$78.0[9.8]$	$22.4[2.8]$	$49[6] \times 10^{-3}$	$17[2] \times 10^{-3}$
	$|g_{\tau R}g_{\mu R}^*\Delta T_{3\psi}|$	$|g_{\tau R}g_{\mu R}^*\kappa_R|$	$|g_{\tau R}g_{\mu R}^*g_{\mu R}g_{\mu R}^*|$	$|g_{\tau R}g_{\mu R}^*g_{\mu L}g_{\mu L}^*|$
$\tau^- \to \mu^-\mu^+\mu^-$	$0.24[0.03]$	$0.03[0.004]$	$8.7\{16.7\}[1.1\{2.1\}]$	$8.1\{8.1\}[1.0\{1.0\}]$
	$|g_{\tau R}g_{eR}^*g_{\mu R}g_{eR}^*|$	$|g_{\tau R}g_{eR}^*g_{\mu L}g_{eL}^*|$	$|g_{\tau R}g_{eL}^*g_{\mu R}g_{eL}^*|$	
$\tau^- \to e^-\mu^+e^-$	$7.4\{14.1\}[0.9\{1.8\}]$	$7.1\{7.1\}[0.9\{0.9\}]$	$31.0\{31.0\}[3.9\{3.9\}]$	
	$|g_{\tau R}g_{\mu R}^*g_{eR}g_{\mu R}^*|$	$|g_{\tau R}g_{\mu R}^*g_{eL}g_{\mu L}^*|$	$|g_{\tau R}g_{\mu L}^*g_{eR}g_{\mu L}^*|$	
$\tau^- \to \mu^-e^+\mu^+$	$7.9\{15.0\}[1.0\{1.9\}]$	$7.5\{7.5\}[0.9\{0.9\}]$	$33.0\{33.0\}[4.2\{4.2\}]$	

source. Our finding agrees with Ref. [27], where a common explanation of Δa_e and Δa_μ was investigated and it was found that the present $\mu \to e\gamma$ bound do not support a common explanation of the deviations.

Presently, the upper limit in $\mu \to e\gamma$ decay gives the most severe constraints on photonic penguin contributions in $\mu \to e$ transitions, agreeing with [79,80], but the situation may change when we include future experimental sensitivities in the analysis. From Tables IV–VI and Figs. 4(a)–4(d), we see that the present $\mu \to e\gamma$ bound constrains the $|Q_{\phi,\psi}g_{\mu R}^* g_{eR}|$ and $|Q_{\phi,\psi}g_{\mu R}^* g_{eL}|$ much better than the present $\mu \to 3e$ and $\mu N \to eN$ upper limits. In fact, the bounds obtained from $\mu \to e\gamma$ decay are better than

those from other processes by at least one order of magnitude. The situation is altered when considering future experimental searches. From the tables and the figures, we see that, on the contrary, in near future experiments the $\mu \to 3e$ and $\mu N \to eN$ processes may be able to probe the photonic penguin contributions from $|Q_{\phi,\psi}g_{\mu R}^* g_{eR}|$ and $|Q_{\phi,\psi}g_{\mu R}^* g_{eL}|$ better than the future experiment search on $\mu \to e\gamma$ decay.

The Z-penguin diagrams can constrain chiral interaction better than photonic penguin diagrams in $\mu \to e$ transitions. From Tables IV–VI, Figs. 4(a), 4(b), 4(e), and 4(f) we see that the bounds on $|g_{\mu R}^* g_{eR}\Delta T_{3\psi}|$ and $|g_{\mu R}^* g_{eR}\kappa_R|$ from Z-penguin contributions are more severe (by two orders of
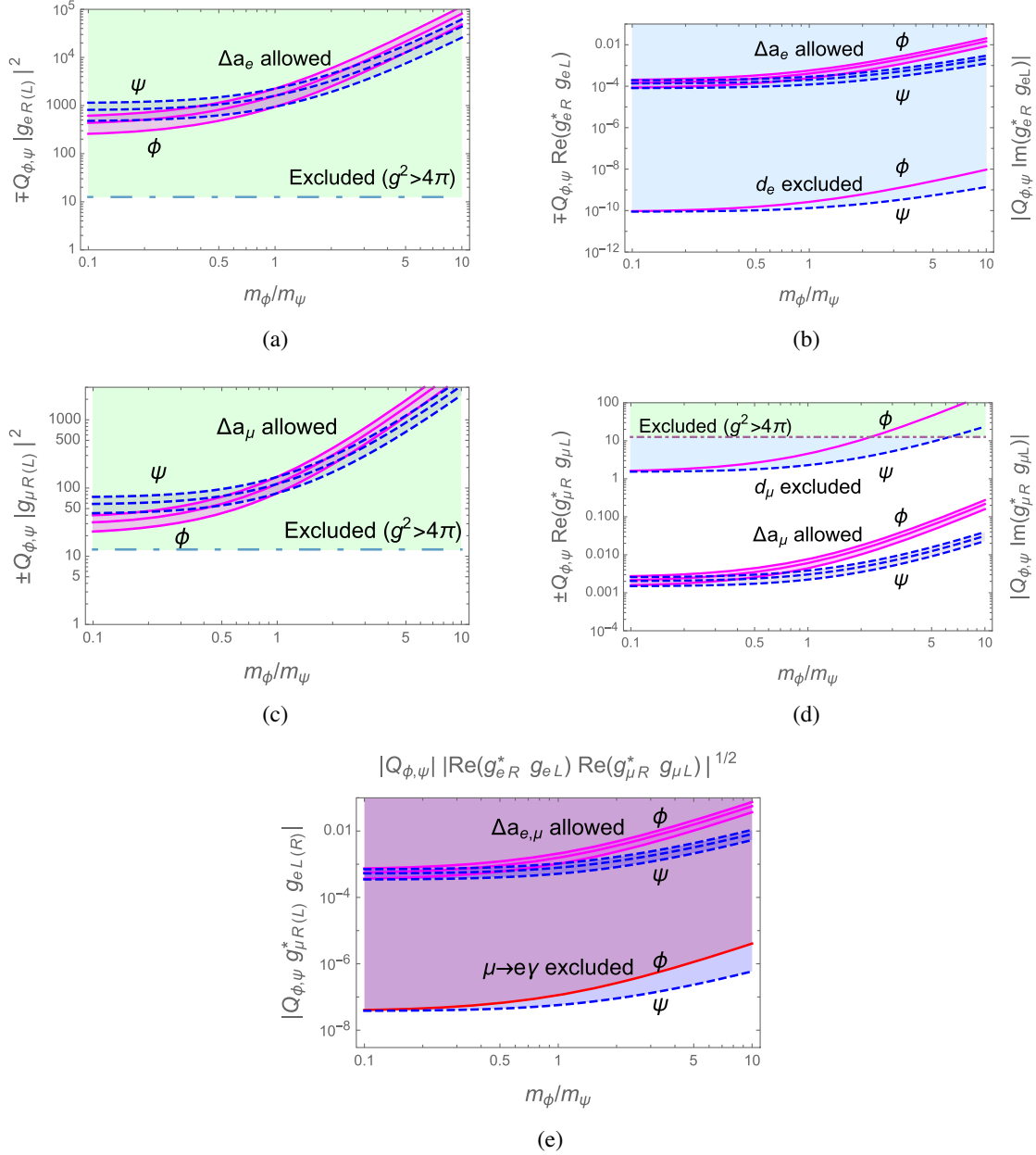
FIG. 3. We show in (a) and (b), allowed parameter space for $\mp Q_{\phi,\psi}|g_{eL(R)}|^2$, $\mp Q_{\phi,\psi}\mathrm{Re}(g_{eR}^* g_{eL})$, and $|Q_{\phi,\psi}\mathrm{Im}(g_{eR}^* g_{eL})|$ constrained by Δa_e and d_e, in (c) and (d), allowed parameter space for $\pm Q_{\phi,\psi}|g_{\mu L(R)}|^2$, $\pm Q_{\phi,\psi}\mathrm{Re}(g_{\mu R}^* g_{\mu L})$, and $|Q_{\phi,\psi}\mathrm{Im}(g_{\mu R}^* g_{\mu L})|$ constrained by Δa_μ and d_μ, in (e) allowed parameter space for $|Q_{\phi,\psi}g_{\mu R(L)}^* g_{eL(R)}|$ constrained by $\mu \to e\gamma$ and the parameter space on $|Q_{\phi,\psi}||\mathrm{Re}(g_{eR}^* g_{eL})\mathrm{Re}(g_{\mu R}^* g_{\mu L})|^{1/2}$ to produce Δa_e and Δa_μ. These results are given for $m_\psi = 500$ GeV. For other m_ψ, plots in (a) and (c) scale with $(500\ \mathrm{GeV}/m_\psi)^2$, while plots in (b), (d) and (e) scale with $500\ \mathrm{GeV}/m_\psi$.

magnitude) than bounds on $|Q_{\phi,\psi}g_{\mu R}^* g_{eR}|$ from photonic penguin contributions. In addition, from Figs. 4(e) and 4(f) we see that $\mu N \to eN$ transitions give better constraints on $|g_{\mu R}^* g_{eR}\Delta T_{3\psi}|$ and $|g_{\mu R}^* g_{eR}\kappa_R|$ than the $\mu \to 3e$ decay.

In case I, either in the Dirac or Majorana case, box contributions to $\mu \to 3e$ decay are subleading. Furthermore, there are cancelation in box contributions in the Majorana fermionic case making the contributions even smaller. Figures 4(g) and 4(h) show the bounds on

$|g_{\mu R}^* g_{eR}g_{eR}^* g_{eR}|$ and $|g_{\mu R}^* g_{eR}g_{eL}^* g_{eL}|$ obtained by considering box contributions to $\mu \to 3e$ decay. Note that the constraint on $|g_{\mu R}^* g_{eR}\Delta T_{3\psi}||g_{eL}^* g_{eL}|$ obtained from $\mu\mathrm{Au} \to e\mathrm{Au}$ upper limit and perturbativity is much severe than the $|g_{\mu R}^* g_{eR}g_{eR}^* g_{eR}|$ bound by one to two orders of magnitude, while $|Q_{\phi,\psi}g_{\mu R}^* g_{eL}||g_{eL}^* g_{eR}|$ obtained from $\mu \to e\gamma$, Δa_e, and d_e experimental results is much severe than the $|g_{\mu R}^* g_{eR}g_{eL}^* g_{eL}|$ bound by more than 8 orders of magnitude. One can also use the values in Tables IV–VI to obtain
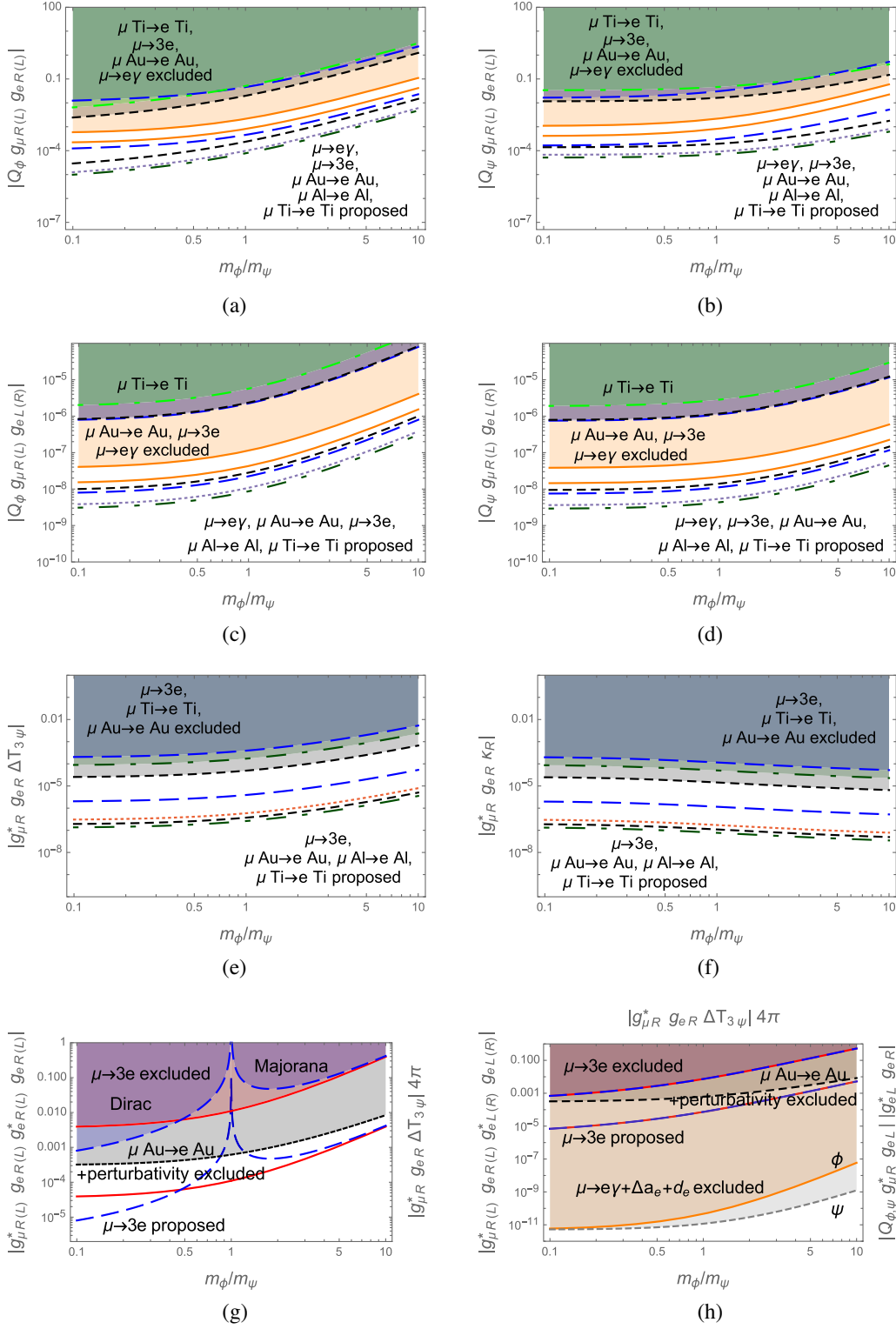
FIG. 4. Parameter space excluded or projected by various experimental bounds or expected sensitivities on $\mu \to e$ LFV processes from photonic penguin, Z-penguin, and box contributions.

similar findings. These results imply that box contributions to $\mu \to 3e$ decay are subleading.

From Tables IV–VI, we see that the present bounds on Δa_τ cannot constrain $Q_{\phi,\psi}|g_{\tau R(L)}|^2$ and $Q_{\phi,\psi}\text{Re}(g_{\tau R}^* g_{\tau L})$

well. Even the bound on d_τ cannot give good constraints on $Q_{\phi,\psi}\text{Im}(g_{\tau R}^* g_{\tau L})$. There is still a long way to go.

In $\tau \to e$ (μ) transitions, the $\tau \to e\gamma$ ($\mu\gamma$) upper limit constrains photonic penguin contributions better than the
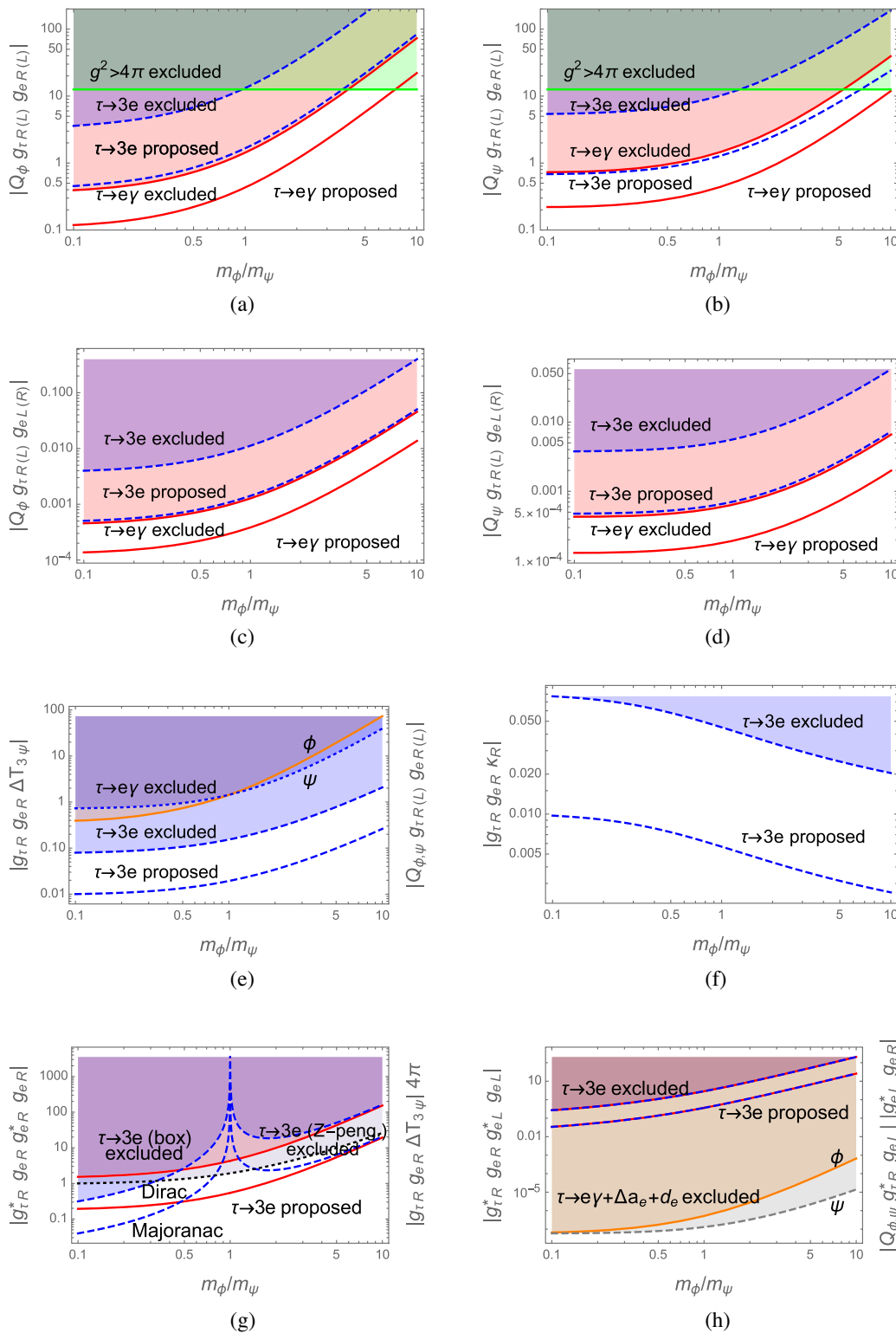
FIG. 5. Same as Fig. 4, but for $\tau \to e$ transition.

$\tau \to 3e$ (3μ) upper limit, agreeing with [80], and Z-penguin constrains chiral interaction better than photonic penguin. From Tables IV–VI, Figs. 5(a)–5(d) and 6(a)–6(d), we see that bounds on $|Q_{\phi,\psi} g^*_{\tau R} g_{e(\mu)R}|$ and $|Q_{\phi,\psi} g^*_{\tau R} g_{e(\mu)L}|$ are constrained by the $\tau \to e\gamma(\mu\gamma)$ data more severely than

by the $\tau \to 3e$ (3μ) upper limit. Note that the bounds of these parameters using the proposed sensitivities on $\tau \to 3e$ and $\tau \to 3\mu$ decays by Belle II are superseded by the bounds using the present limits of $\tau \to e\gamma$ and $\tau \to \mu\gamma$ decays. From Tables IV–VI, Figs. 5(e), 5(f), 6(e),
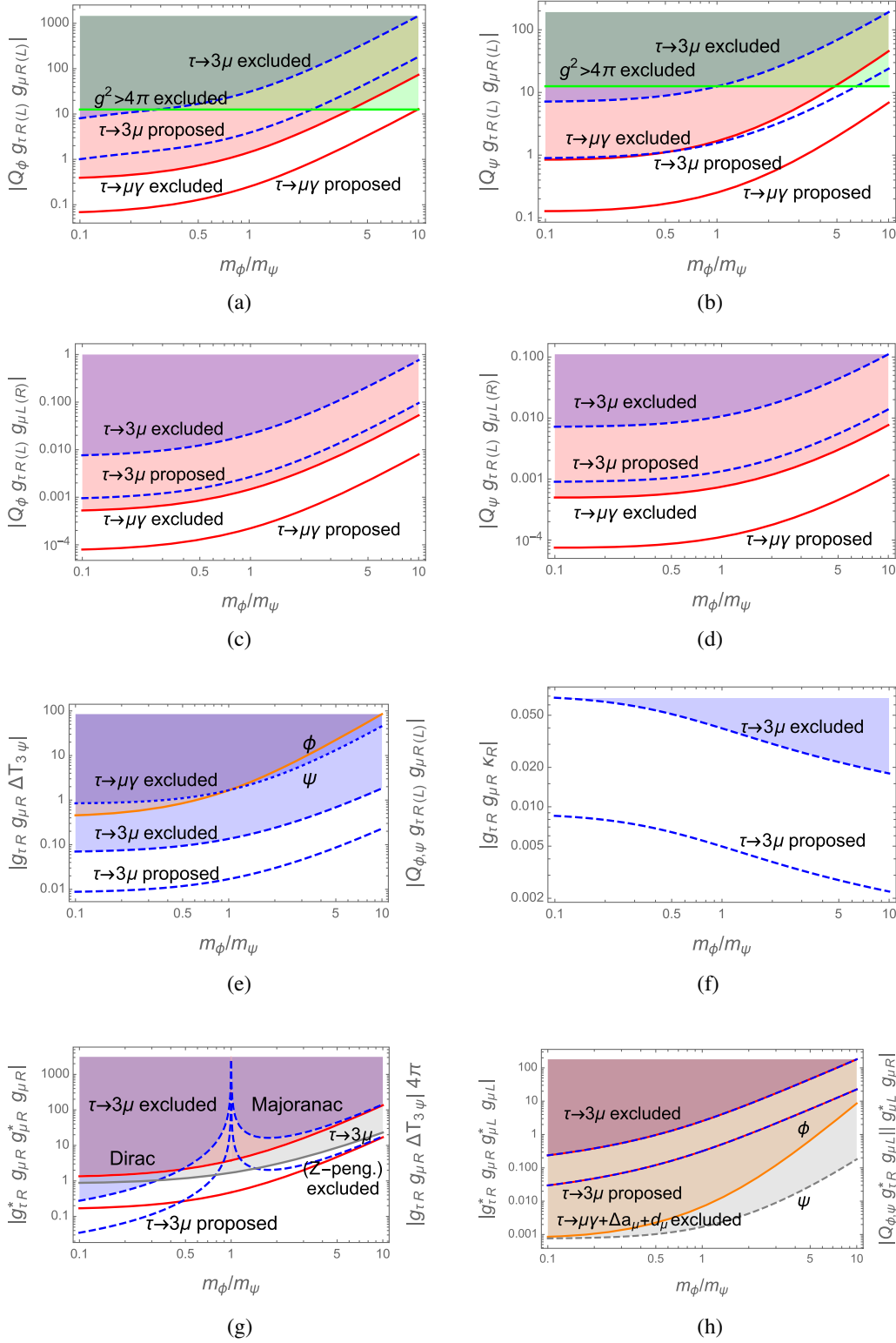
FIG. 6. Same as Fig. 4, but for $\tau \to \mu$ transition.

and 6(f), we see that bounds on $|g_{\tau R}^* g_{e(\mu)R} \Delta T_{3\psi}|$ and $|g_{\tau R}^* g_{e(\mu)R} \kappa_R|$ from Z-penguin contributions are more severe (by one order of magnitude) than those on $|Q_{\phi,\psi} g_{\tau R}^* g_{e(\mu)R}|$ from photonic penguin contributions.

Hence, Z-penguin constrains chiral interaction better than photonic penguin.

Box contributions to $\tau \to 3e$ and $\tau \to 3\mu$ decays can sometime be comparable to Z-penguin contributions.
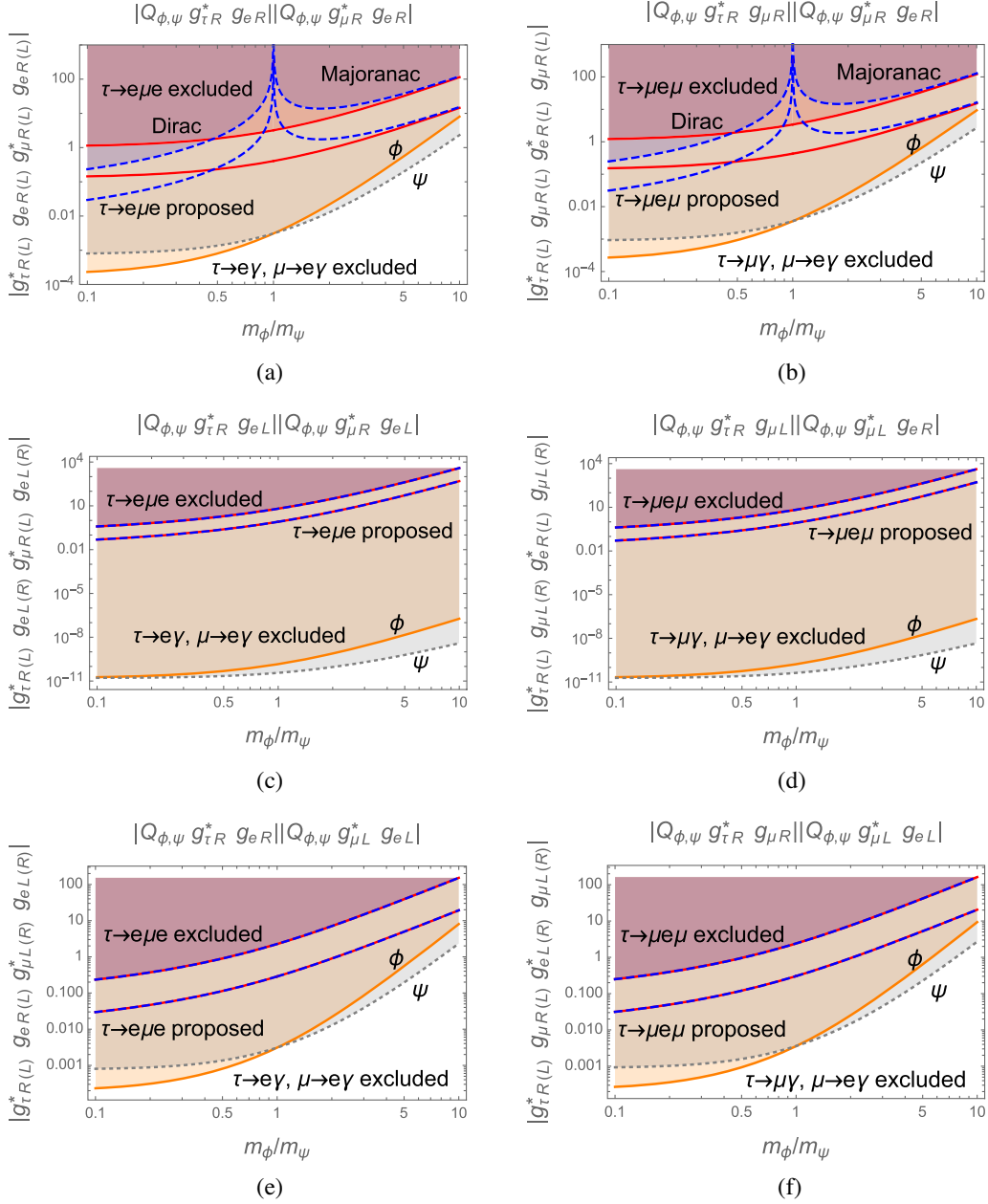
FIG. 7. Parameter space excluded or projected by various experimental bounds or expected sensitivities on $\tau^- \to e^- \mu^+ e^-, \mu^- e^+ \mu^-$ processes from box contributions.

In Figs. 5(g), 5(h), 6(g), and 6(h) we show the bounds on $|g^*_{\tau R} g_{e(\mu)R} g^*_{e(\mu)R} g_{e(\mu)R}|$ and $|g^*_{\tau R} g_{e(\mu)R} g^*_{e(\mu)L} g_{e(\mu)L}|$ obtained by considering box contributions to $\tau \to 3e$ (3μ) decay. Note that the constraint on $|g^*_{\tau R} g_{e(\mu)R} \Delta T_{3\psi}||g^*_{e(\mu)L} g_{e(\mu)L}|$ obtained from Z-penguin contributions to $\tau \to 3e$ (3μ) decay and perturbativity is much severe than the $|g^*_{\tau R} g_{e(\mu)R} g^*_{e(\mu)R} g_{e(\mu)R}|$ bound from box contributions for $x \gtrsim 0.4$, but it is the other way around for $x \lesssim 0.4$. The bound on $|Q_{\phi,\psi} g^*_{\tau R} g_{e(\mu)L}||g^*_{e(\mu)L} g_{e(\mu)R}|$ obtained using $\tau \to e\gamma(\mu\gamma)$, $\Delta a_{e(\mu)}$ and $d_{e(\mu)}$ experimental results is much severe than the $|g^*_{\tau R} g_{e(\mu)R} g^*_{e(\mu)L} g_{e(\mu)L}|$ bound from box

contributions by five to seven (one to three) orders of magnitude. One can also obtain similar results using the values in Tables IV–VI. These findings imply that box contributions to $\tau \to 3e$ (3μ) can sometime be comparable to Z-penguin contributions.

The $\tau^- \to e^- \mu^+ e^-$ rate is highly constrained by $\tau \to e\gamma$ and $\mu \to e\gamma$ upper limits. From Figs. 7(a), 7(c), and 7(e), Tables IV–VI, we see that the bounds on $|g^*_{\tau R} g_{eR} g^*_{\mu R} g_{eR}|$, $|g^*_{\tau R} g_{eL} g^*_{\mu R} g_{eL}|$, and $|g^*_{\tau R} g_{eR} g^*_{\mu L} g_{eL}|$, obtained from the upper limit of the $\tau^- \to e^- \mu^+ e^-$ rate, are larger than the bounds on $|Q_{\phi,\psi} g^*_{\tau R} g_{eR}||Q_{\phi,\psi} g^*_{\mu R} g_{eR}|$, $|Q_{\phi,\psi} g^*_{\tau R} g_{eL}||Q_{\phi,\psi} g^*_{\mu R} g_{eL}|$, and $|Q_{\phi,\psi} g^*_{\tau R} g_{eR}||Q_{\phi,\psi} g^*_{\mu L} g_{eL}|$, obtained from the upper limits

TABLE VII.   Current experimental upper limits, future sensitivities and bounds from consistency in case I on various muon and tau LFV processes. Experimental bounds are from [4,17,22–24].

	Current limit (future sensitivity)	Consistency bounds	Remarks
$\mathcal{B}(\mu^+ \to e^+\gamma)$	$<4.2 \times 10^{-13}$ (6×10^{-14})	$<4.2 \times 10^{-13}$	Input
$\mathcal{B}(\mu^+ \to e^+e^+e^-)$	$<1.0 \times 10^{-12}$ (10^{-16})	$<1.3 \times 10^{-14}$	From $\mu \to e\gamma$ bound
		$<1.6 \times 10^{-14}$	From $\mu\text{Au} \to e\text{Au}$ bound
$\mathcal{B}(\mu^-\text{Ti} \to e^-\text{Ti})$	$<4.3 \times 10^{-12}$ (10^{-17})	$<9.1 \times 10^{-14}$	From $\mu \to e\gamma$ bound
		$<3.5 \times 10^{-13}$	From $\mu\text{Au} \to e\text{Au}$ bound
$\mathcal{B}(\mu^-\text{Au} \to e^-\text{Au})$	$<7.0 \times 10^{-13}$ (10^{-16})	$<1.1 \times 10^{-13}$	From $\mu \to e\gamma$ bound
		$<7.0 \times 10^{-13}$	Input
$\mathcal{B}(\mu^-\text{Al} \to e^-\text{Al})$	$\cdots$ (10^{-17})	$<5.5 \times 10^{-14}$	From $\mu \to e\gamma$ bound
		$<1.7 \times 10^{-13}$	From $\mu\text{Au} \to e\text{Au}$ bound
$\mathcal{B}(\tau^- \to e^-\gamma)$	$<3.3 \times 10^{-8}$ (3×10^{-9})	$<3.3 \times 10^{-8}$	Input
$\mathcal{B}(\tau^- \to e^-e^+e^-)$	$<2.7 \times 10^{-8}$ (4.3×10^{-10})	$<1.2 \times 10^{-9}$	From $\tau \to e\gamma$ bound
$\mathcal{B}(\tau^- \to \mu^-\gamma)$	$<4.4 \times 10^{-8}$ (1×10^{-9})	$<4.4 \times 10^{-8}$	Input
$\mathcal{B}(\tau^- \to \mu^-\mu^+\mu^-)$	$<2.1 \times 10^{-8}$ (3.3×10^{-10})	$<1.2 \times 10^{-9}$	From $\tau \to \mu\gamma$ bound
$\mathcal{B}(\tau^- \to \mu^-e^+\mu^-)$	$<1.7 \times 10^{-8}$ (2.7×10^{-10})	$\lesssim 1 \times 10^{-10}$	From $\tau \to \mu\gamma$, $\mu \to e\gamma$ bounds
$\mathcal{B}(\tau^- \to e^-\mu^+e^-)$	$<1.5 \times 10^{-8}$ (2.4×10^{-10})	$\lesssim 7 \times 10^{-11}$	From $\tau \to e\gamma$, $\mu \to e\gamma$ bounds

of $\tau \to e\gamma$ and $\mu \to e\gamma$ rates, by several orders of magnitude. Note that the $\tau^- \to e^-\mu^+e^-$ rate is constrained to be smaller than the proposed sensitivity. Hence, the $\tau^- \to e^-\mu^+e^-$ rate is highly constrained by the present $\tau \to e\gamma$ and $\mu \to e\gamma$ upper limits.

The $\tau^- \to \mu^-e^+\mu^-$ rate is also highly constrained by $\tau \to \mu\gamma$ and $\mu \to e\gamma$ upper limits. From Figs. 7(b), 7(d), and 7(f), Tables IV–VI, we see that the bounds on $|g_{\tau R}^* g_{\mu R} g_{eR}^* g_{\mu R}|$, $|g_{\tau R}^* g_{\mu L} g_{eR}^* g_{\mu L}|$, and $|g_{\tau R}^* g_{\mu R} g_{eL}^* g_{\mu L}|$, obtained from the upper limit of the $\tau^- \to \mu^-e^+\mu^-$ rate, are larger than the bounds on $|Q_{\phi,\psi} g_{\tau R}^* g_{\mu R}||Q_{\phi,\psi} g_{\mu R}^* g_{eR}|$, $|Q_{\phi,\psi} g_{\tau R}^* g_{\mu L}||Q_{\phi,\psi} g_{\mu L}^* g_{eR}|$, and $|Q_{\phi,\psi} g_{\tau R}^* g_{\mu R}||Q_{\phi,\psi} g_{\mu L}^* g_{eL}|$, obtained from the upper limits of $\tau \to e\gamma$ and $\mu \to e\gamma$ rates, by several orders of magnitude. Hence, the $\tau^- \to \mu^-e^+\mu^-$ rate is highly constrained by $\tau \to \mu\gamma$ and $\mu \to e\gamma$ upper limits. In fact, the $\tau^- \to \mu^-e^+\mu^-$ rate is constrained to be smaller than the proposed sensitivity.

In Table VII, we compare the current experimental upper limits, future sensitivities and bounds from consistency for case I on various muon and tau LFV processes. We see that the present $\mu \to e\gamma$ upper limit requires the bounds on $\mu \to 3e$, $\mu\text{Ti} \to e\text{Ti}$ and $\mu\text{Au} \to e\text{Au}$ be lower by two orders of magnitude, more than one order of magnitude and almost one order of magnitude, respectively, from their present upper limits, and the $\mu\text{Al} \to e\text{Al}$ rate is predicted to be smaller than 6×10^{-14}. These bounds can be further pushed downward by one order of magnitude if we still cannot observe $\mu \to e\gamma$ decay in MEG II. It is interesting that the future sensitivities of $\mu \to 3e$ and $\mu N \to eN$ are much lower than the above limits based on consistency, giving them good opportunity to explore these LFV processes. We find that the situation is similar but the bounds are slightly relaxed when the $\mu\text{Au} \to e\text{Au}$ upper limit instead of the present $\mu \to e\gamma$ upper limit is used as an input. Similarly, using the present $\tau \to e\gamma(\mu\gamma)$ upper limit

as input, the $\tau \to 3e$ (3μ) bound is smaller than its present upper limit by one order of magnitude. Note that the $\mathcal{B}(l' \to l\bar{l}l)/\mathcal{B}(l' \to l\gamma)$ ratios are close to the values shown in Eq. (8) [79,80], but not identical to them, as the F_1 terms in photonic penguins also play some roles. Finally, the $\tau^- \to \mu^-e^+\mu^-$ and $\tau^- \to e^-\mu^+e^-$ bounds are lower than their present upper limits by two orders of magnitude as required from the present $\tau \to \mu\gamma$, $e\gamma$ and $\mu \to e\gamma$ upper limits. These limits are lower than the proposed future sensitivities.

B. Case II

We now turn to the second case, where we have a built-in cancellation mechanism.

In Table VIII, we show the constraints on parameters in case II using $x \equiv m_\phi/m_\psi = 1$ and $m_\psi = 500$ GeV. Constraints for other m_ψ can be obtained by scaling the results in the table by a $\left(\frac{m_\psi}{500 \text{ GeV}}\right)^2$ or a $\frac{m_\psi}{500 \text{ GeV}}$ factor, where the latter is for $Q_{\phi,\psi} g_{l^{(\prime)}R}^* g_{lL}$. Results in [...] are obtained by using the projected sensitivities for future experiments. For box contributions both results of Dirac and Majorana fermion are given, where results in {...} are for the Majorana case. Results for $x = 0.5$ and 2 are given in Tables IX and X, respectively.

In Fig. 8, the allowed parameter space for (a) $\pm Q_{\phi,\psi} \times \text{Re}(g_{eR}^* g_{eL} \delta_{RL}^{ee})$ and $|Q_{\phi,\psi}\text{Im}(g_{eR}^* g_{eL} \delta_{RL}^{ee})|$ constrained by Δa_μ and d_e, respectively, and (b) $\mp Q_{\phi,\psi}\text{Re}(g_{\mu R}^* g_{\mu L} \delta_{RL}^{\mu\mu})$ and $|Q_{\phi,\psi}\text{Im}(g_{\mu R}^* g_{\mu L} \delta_{RL}^{\mu\mu})|$ constrained by Δa_μ and d_μ, respectively, are shown. These constraints are obtained using $m_\psi = 500$ GeV. For other m_ψ, apply a $(500 \text{ GeV})/m_\psi$ factor to the plots.

In Figs. 9–11, we show the parameter space constrained by using various experimental bounds or expected sensitivities on $\mu \to e$, $\tau \to e$ and $\tau \to \mu$ lepton flavor violating processes. Contributions from photonic penguin,

TABLE VIII. Same as Table IV ($x = 1$), but for case II.

Processes	Constraints	Constraints	Constraints	Constraints
Δa_e	$Q_\phi|g_{eR}|^2$ -1597 ± 653	$Q_\psi|g_{eR}|^2$ 1597 ∓ 653	$Q_\phi\mathrm{Re}(g_{eR}^*g_{eL}\delta_{RL}^{ee})$ $(8 \mp 3) \times 10^{-4}$	$Q_\psi\mathrm{Re}(g_{eR}^*g_{eL}\delta_{RL}^{ee})$ $(-8 \pm 3) \times 10^{-4}$
Δa_μ	$Q_\phi|g_{\mu R}|^2$ 115 ± 31	$Q_\psi|g_{\mu R}|^2$ -115 ∓ 31	$Q_\phi\mathrm{Re}(g_{\mu R}^*g_{\mu L}\delta_{RL}^{\mu\mu})$ $(-12 \mp 3) \times 10^{-3}$	$Q_\psi\mathrm{Re}(g_{\mu R}^*g_{\mu L}\delta_{RL}^{\mu\mu})$ $(-12 \pm 3) \times 10^{-3}$
Δa_τ	$Q_\phi|g_{\tau R}|^2$ $(-7 \sim 2) \times 10^6$	$Q_\psi|g_{\tau R}|^2$ $(-2 \sim 7) \times 10^6$	$Q_\phi\mathrm{Re}(g_{\tau R}^*g_{\tau L}\delta_{RL}^{\tau\tau})$ $(-3 \sim 13) \times 10^3$	$Q_\psi\mathrm{Re}(g_{\tau R}^*g_{\tau L}\delta_{RL}^{\tau\tau})$ $(-13 \sim 3) \times 10^3$
d_e, d_μ, d_τ	$|Q_\phi\mathrm{Im}(g_{eR}^*g_{eL}\delta_{RL}^{ee})|$ 5.3×10^{-10}	$|Q_\phi\mathrm{Im}(g_{eR}^*g_{eL})\delta_{RL}^{ee}|$ 5.3×10^{-10}	$|Q_\phi\mathrm{Im}(g_{lR}^*g_{lL}\delta_{RL}^{ll})|_{l=\mu(\tau)}$ $9.1(76.5)$	$|Q_\psi\mathrm{Im}(g_{lR}^*g_{lL}\delta_{RL}^{ll})|_{l=\mu(\tau)}$ $9.1(76.5)$
	$|Q_\phi g_{\mu R}^*g_{eR}\delta_{RR}^{\mu e}|$	$|Q_\psi g_{\mu R}^*g_{eR}\delta_{RR}^{\mu e}|$	$|Q_\phi g_{\mu R}^*g_{eL}\delta_{RL}^{\mu e}|$	$|Q_\psi g_{\mu R}^*g_{eL}\delta_{RL}^{\mu e}|$
$\mu^+ \to e^+\gamma$	0.004[0.0014]	0.005[0.0020]	$23[9] \times 10^{-8}$	$23[9] \times 10^{-8}$
$\mu^+ \to e^-e^+e^-$	0.077[0.0008]	0.085[0.0008]	$448[4] \times 10^{-8}$	$448[4] \times 10^{-8}$
$\mu^-\mathrm{Au} \to e^-\mathrm{Au}$	0.028[0.0003]	0.074[0.0009]	$471[6] \times 10^{-8}$	$471[6] \times 10^{-8}$
$\mu^-\mathrm{Ti} \to e^-\mathrm{Ti}$	0.072[0.0001]	0.219[0.0003]	$1137[2] \times 10^{-8}$	$1137[2] \times 10^{-8}$
$\mu^-\mathrm{Al} \to e^-\mathrm{Al}$	[0.0001]	[0.0004]	$[2 \times 10^{-8}]$	$[2 \times 10^{-8}]$
	$|g_{\mu R}^*g_{eR}\Delta T_{3\psi}\delta_{RR}^{\mu e}|$	$|g_{\mu R}^*g_{eR}g_{eR}^*g_{eR}\delta_{RR}^{\mu e}|$	$|g_{\mu R}^*g_{eR}g_{eL}^*g_{eL}\delta_{RR}^{\mu e}|$	
$\mu^+ \to e^-e^+e^-$	$118[1] \times 10^{-5}$	$0.04\{0.04\}[4\{4\} \times 10^{-4}]$	$0.03\{0.06\}[3\{6\} \times 10^{-4}]$	
$\mu^-\mathrm{Au} \to e^-\mathrm{Au}$	$148[2] \times 10^{-6}$			
$\mu^-\mathrm{Ti} \to e^-\mathrm{Ti}$	$5155[8] \times 10^{-7}$			
$\mu^-\mathrm{Al} \to e^-\mathrm{Al}$	$[1 \times 10^{-6}]$			
	$|Q_\phi g_{\tau R}g_{eR}^*\delta_{RR}^{e\tau}|$	$|Q_\psi g_{\tau R}g_{eR}^*\delta_{RR}^{e\tau}|$	$|Q_\phi g_{\tau R}g_{eL}^*\delta_{LR}^{e\tau}|$	$|Q_\psi g_{\tau R}g_{eL}^*\delta_{LR}^{e\tau}|$
$\tau^- \to e^-\gamma$	2.4[0.7]	3.6[1.1]	$26[8] \times 10^{-4}$	$26[8] \times 10^{-4}$
$\tau^- \to e^-e^+e^-$	22.2[2.8]	27.3[3.5]	$22[3] \times 10^{-3}$	$22[3] \times 10^{-3}$
	$|g_{\tau R}g_{eR}^*\Delta T_{3\psi}\delta_{RR}^{e\tau}|$	$|g_{\tau R}g_{eR}^*g_{eR}g_{eR}^*\delta_{RR}^{e\tau}|$	$|g_{\tau R}g_{eR}^*g_{eL}g_{eL}^*\delta_{RR}^{e\tau}|$	
$\tau^- \to e^-e^+e^-$	0.46[0.06]	$17.2\{17.2\}[2.2\{2.2\}]$	$12.2\{24.3\}[1.5\{3.1\}]$	
	$|Q_\phi g_{\tau R}g_{\mu R}^*\delta_{RR}^{\mu\tau}|$	$|Q_\psi g_{\tau R}g_{\mu R}^*\delta_{RR}^{\mu\tau}|$	$|Q_\phi g_{\tau R}g_{\mu L}^*\delta_{LR}^{\mu\tau}|$	$|Q_\psi g_{\tau R}g_{\mu R}^*\delta_{LR}^{\mu\tau}|$
$\tau^- \to \mu^-\gamma$	2.8[0.4]	4.2[0.6]	$30[4] \times 10^{-4}$	$30[4] \times 10^{-4}$
$\tau^- \to \mu^-\mu^+\mu^-$	19.5[2.4]	24.1[3.0]	$20[2] \times 10^{-3}$	$20[2] \times 10^{-3}$
	$|g_{\tau R}g_{\mu R}^*\Delta T_{3\psi}\delta_{RR}^{\mu\tau}|$	$|g_{\tau R}g_{\mu R}^*g_{\mu R}g_{\mu R}^*\delta_{RR}^{\mu\tau}|$	$|g_{\tau R}g_{\mu R}^*g_{\mu L}g_{\mu L}^*\delta_{RR}^{\mu\tau}|$	
$\tau^- \to \mu^-\mu^+\mu^-$	0.41[0.05]	$15.2\{15.2\}[1.9\{1.9\}]$	$10.7\{21.4\}[1.3\{2.7\}]$	
	$|g_{\tau R}g_{eR}^*g_{\mu R}g_{eR}^*\delta_{RR}^{e\tau}\delta_{RR}^{e\mu}|$	$|g_{\tau R}g_{eR}^*g_{\mu L}g_{eL}^*\delta_{RR}^{e\tau}\delta_{LL}^{e\mu}|$	$|g_{\tau R}g_{eL}^*g_{\mu R}g_{eL}^*\delta_{LR}^{e\tau}\delta_{LR}^{e\mu}|$	$|g_{\tau R}g_{eL}^*g_{\mu L}g_{eR}^*\delta_{LR}^{e\tau}\delta_{RL}^{e\mu}|$
$\tau^- \to e^-\mu^+e^-$	$32.0\{16.0\}[4.1\{2.0\}]$	$15.1\{22.7\}[1.9\{2.9\}]$	$21.4\{21.4\}[2.7\{2.7\}]$	$45.3\{22.7\}[5.7\{2.9\}]$
	$|g_{\tau R}g_{\mu R}^*g_{eR}g_{\mu R}^*\delta_{RR}^{\mu\tau}\delta_{RR}^{\mu e}|$	$|g_{\tau R}g_{\mu R}^*g_{eL}g_{\mu L}^*\delta_{RR}^{\mu\tau}\delta_{LL}^{\mu e}|$	$|g_{\tau R}g_{\mu L}^*g_{eR}g_{\mu L}^*\delta_{LR}^{\mu\tau}\delta_{LR}^{\mu e}|$	$|g_{\tau R}g_{\mu L}^*g_{eL}g_{\mu R}^*\delta_{LR}^{\mu\tau}\delta_{RL}^{\mu e}|$
$\tau^- \to \mu^-e^+\mu^+$	$34.1\{17.1\}[4.3\{2.1\}]$	$16.1\{24.1\}[2.0\{3.0\}]$	$22.7\{22.7\}[2.9\{2.9\}]$	$48.2\{24.1\}[6.1\{3.0\}]$

Z-penguin, and box diagrams are considered. In Fig. 12, the parameter space constrained by using various bounds or expected experimental sensitivities on $\tau^- \to e^-\mu^+e^-$, $\mu^-e^+\mu^-$ processes through contributions from box contributions are shown.

There are several messages we can extracted from these results. First we note that, comparing to case I, the built-in cancellation has more prominent effects in penguin amplitudes than in box amplitudes. Furthermore, the cancellation affects small-x ($x \equiv m_\phi/m_\psi$) region more effectively. We can see this clearly in the above figures by noting that the curves corresponding to penguin contributions bend upward in the small-x region, hence, relaxing the constraints.

Similar to case I, we note that chiral interactions ($g_L \times g_R = 0$) are unable to generate large enough contributions to Δa_e and Δa_μ to accommodate the experimental results, Eqs. (1) and (2). This can be seen in Tables IV, IX, and X, where $Q_{\phi,\psi}|g_{eR(L)}|^2$ and $Q_{\phi,\psi}|g_{\mu R(L)}|^2$ need to be unreasonably and unacceptably large to produce the experimental values of Δa_e and Δa_μ.

Again similar to case I, we find that although nonchiral interactions are capable to generate Δa_e and Δa_μ successfully accommodating the experimental results, they are contributed from different sources. From Tables VIII–X, we see that $Q_{\phi,\psi}\mathrm{Re}(g_{eR}^*g_{eL}\delta_{RL}^{ee})$ and $Q_{\phi,\psi}\mathrm{Re}(g_{\mu R}^*g_{\mu L}\delta_{RL}^{\mu\mu})$ of orders 10^{-3} and 10^{-2} or larger, are able to produce the

TABLE IX. Same as Table VIII, but with $x \equiv m_\phi/m_\psi = 0.5$.

Processes	Constraints	Constraints	Constraints	Constraints
Δa_e	$Q_\phi\lvert g_{eR}\rvert^2$ -812 ± 332	$Q_\psi\lvert g_{eR}\rvert^2$ 1059 ∓ 433	$Q_\phi\mathrm{Re}(g_{eR}^*g_{eL}\delta_{RL}^{ee})$ $(8 \mp 3)\times10^{-4}$	$Q_\psi\mathrm{Re}(g_{eR}^*g_{eL}\delta_{RL}^{ee})$ $(-13 \pm 6)\times10^{-4}$
Δa_μ	$Q_\phi\lvert g_{\mu R}\rvert^2$ 58 ± 16	$Q_\psi\lvert g_{\mu R}\rvert^2$ -76 ∓ 20	$Q_\phi\mathrm{Re}(g_{\mu R}^*g_{\mu L}\delta_{RL}^{\mu\mu})$ $(-1.2 \mp 0.3)\times10^{-2}$	$Q_\psi\mathrm{Re}(g_{\mu R}^*g_{\mu L}\delta_{RL}^{\mu\mu})$ $(-20 \pm 5)\times10^{-3}$
Δa_τ	$Q_\phi\lvert g_{\tau R}\rvert^2$ $(-4\sim1)\times10^6$	$Q_\psi\lvert g_{\tau R}\rvert^2$ $(-1\sim5)\times10^6$	$Q_\phi\mathrm{Re}(g_{\tau R}^*g_{\tau L}\delta_{RL}^{\tau\tau})$ $(-3\sim13)\times10^3$	$Q_\psi\mathrm{Re}(g_{\tau R}^*g_{\tau L}\delta_{RL}^{\tau\tau})$ $(-22\sim5)\times10^3$
d_e, d_μ, d_τ	$\lvert Q_\phi\mathrm{Im}(g_{eR}^*g_{eL}\delta_{RL}^{ee})\rvert$ 5.0×10^{-10}	$\lvert Q_\phi\mathrm{Im}(g_{eR}^*g_{eL})\delta_{RL}^{ee}\rvert$ 8.7×10^{-10}	$\lvert Q_\phi\mathrm{Im}(g_{lR}^*g_{lL}\delta_{RL}^{ll})\rvert_{l=\mu(\tau)}$ $8.7(73.0)$	$\lvert Q_\psi\mathrm{Im}(g_{lR}^*g_{lL}\delta_{RL}^{ll})\rvert_{l=\mu(\tau)}$ $15.0(126.2)$
	$\lvert Q_\phi g_{\mu R}^*g_{eR}\delta_{RR}^{\mu e}\rvert$	$\lvert Q_\psi g_{\mu R}^*g_{eR}\delta_{RR}^{\mu e}\rvert$	$\lvert Q_\phi g_{\mu R}^*g_{eL}\delta_{RL}^{\mu e}\rvert$	$\lvert Q_\psi g_{\mu R}^*g_{eL}\delta_{RL}^{\mu e}\rvert$
$\mu^+ \to e^+\gamma$	$0.003[0.0011]$	$0.007[0.0027]$	$22[8]\times10^{-8}$	$4[1]\times10^{-7}$
$\mu^+ \to e^-e^+e^-$	$0.063[0.0006]$	$0.115[0.0011]$	$427[4]\times10^{-8}$	$739[7]\times10^{-8}$
$\mu^-\mathrm{Au} \to e^-\mathrm{Au}$	$0.015[0.0002]$	$0.136[0.0016]$	$449[5]\times10^{-8}$	$777[9]\times10^{-8}$
$\mu^-\mathrm{Ti} \to e^-\mathrm{Ti}$	$0.040[0.00006]$	$0.416[0.0006]$	$1084[2]\times10^{-8}$	$1875[3]\times10^{-8}$
$\mu^-\mathrm{Al} \to e^-\mathrm{Al}$	$[0.00001]$	$[0.0008]$	$[2\times10^{-8}]$	$[4\times10^{-8}]$
	$\lvert g_{\mu R}^*g_{eR}\Delta T_{3\psi}\delta_{RR}^{\mu e}\rvert$	$\lvert g_{\mu R}^*g_{eR}g_{eR}^*g_{eR}\delta_{RR}^{\mu e}\rvert$	$\lvert g_{\mu R}^*g_{eR}g_{eL}^*g_{eL}\delta_{RR}^{\mu e}\rvert$	
$\mu^+ \to e^-e^+e^-$	$142[1]\times10^{-5}$	$0.04\{0.01\}[4\{1\}\times10^{-4}]$	$0.01\{0.02\}[1\{2\}\times10^{-4}]$	
$\mu^-\mathrm{Au} \to e^-\mathrm{Au}$	$178[2]\times10^{-6}$			
$\mu^-\mathrm{Ti} \to e^-\mathrm{Ti}$	$6226[9]\times10^{-7}$			
$\mu^-\mathrm{Al} \to e^-\mathrm{Al}$	$[1\times10^{-6}]$			
	$\lvert Q_\phi g_{\tau R}g_{eR}^*\delta_{RR}^{e\tau}\rvert$	$\lvert Q_\psi g_{\tau R}g_{eR}^*\delta_{RR}^{e\tau}\rvert$	$\lvert Q_\phi g_{\tau R}g_{eL}^*\delta_{LR}^{e\tau}\rvert$	$\lvert Q_\psi g_{\tau R}g_{eL}^*\delta_{LR}^{e\tau}\rvert$
$\tau^- \to e^-\gamma$	$1.9[0.6]$	$4.7[1.4]$	$24[7]\times10^{-4}$	$42[13]\times10^{-4}$
$\tau^- \to e^-e^+e^-$	$18.0[2.3]$	$36.8[4.6]$	$21[3]\times10^{-3}$	$37[5]\times10^{-3}$
	$\lvert g_{\tau R}g_{eR}^*\Delta T_{3\psi}\delta_{RR}^{e\tau}\rvert$	$\lvert g_{\tau R}g_{eR}^*g_{eR}g_{eR}^*\delta_{RR}^{e\tau}\rvert$	$\lvert g_{\tau R}g_{eR}^*g_{eL}g_{eL}^*\delta_{RR}^{e\tau}\rvert$	
$\tau^- \to e^-e^+e^-$	$0.56[0.07]$	$16.4\{4.5\}[2.1\{0.6\}]$	$5.0\{6.4\}[0.6\{0.8\}]$	
	$\lvert Q_\phi g_{\tau R}g_{\mu R}^*\delta_{RR}^{\mu\tau}\rvert$	$\lvert Q_\psi g_{\tau R}g_{\mu R}^*\delta_{RR}^{\mu\tau}\rvert$	$\lvert Q_\phi g_{\tau R}g_{\mu L}^*\delta_{LR}^{\mu\tau}\rvert$	$\lvert Q_\psi g_{\tau R}g_{\mu L}^*\delta_{LR}^{\mu\tau}\rvert$
$\tau^- \to \mu^-\gamma$	$2.2[0.3]$	$5.4[0.8]$	$28[4]\times10^{-4}$	$49[7]\times10^{-4}$
$\tau^- \to \mu^-\mu^+\mu^-$	$15.8[2.0]$	$32.4[4.1]$	$18[2]\times10^{-3}$	$33[4]\times10^{-3}$
	$\lvert g_{\tau R}g_{\mu R}^*\Delta T_{3\psi}\delta_{RR}^{\mu\tau}\rvert$	$\lvert g_{\tau R}g_{\mu R}^*g_{\mu R}g_{\mu R}^*\delta_{RR}^{\mu\tau}\rvert$	$\lvert g_{\tau R}g_{\mu R}^*g_{\mu L}g_{\mu L}^*\delta_{RR}^{\mu\tau}\rvert$	
$\tau^- \to \mu^-\mu^+\mu^-$	$0.49[0.06]$	$14.4\{4.0\}[1.8\{0.5\}]$	$4.4\{5.6\}[0.6\{0.7\}]$	
	$\lvert g_{\tau R}g_{eR}^*g_{\mu R}g_{eR}^*\delta_{RR}^{e\tau}\delta_{RR}^{e\mu}\rvert$	$\lvert g_{\tau R}g_{eR}^*g_{\mu L}g_{eL}^*\delta_{RR}^{e\tau}\delta_{LL}^{e\mu}\rvert$	$\lvert g_{\tau R}g_{eL}^*g_{\mu R}g_{eL}^*\delta_{LR}^{e\tau}\delta_{LR}^{e\mu}\rvert$	$\lvert g_{\tau R}g_{eL}^*g_{\mu L}g_{eR}^*\delta_{LR}^{e\tau}\delta_{RL}^{e\mu}\rvert$
$\tau^- \to e^-\mu^+e^-$	$41.9\{6.1\}[6.3\{0.8\}]$	$7.5\{8.6\}[1.0\{1.1\}]$	$10.7\{10.7\}[1.3\{1.3\}]$	$59.3\{29.6\}[7.5\{3.7\}]$
	$\lvert g_{\tau R}g_{\mu R}^*g_{eR}g_{\mu R}^*\delta_{RR}^{\mu\tau}\delta_{RR}^{\mu e}\rvert$	$\lvert g_{\tau R}g_{\mu R}^*g_{eL}g_{\mu L}^*\delta_{RR}^{\mu\tau}\delta_{LL}^{\mu e}\rvert$	$\lvert g_{\tau R}g_{\mu L}^*g_{eR}g_{\mu L}^*\delta_{LR}^{\mu\tau}\delta_{LR}^{\mu e}\rvert$	$\lvert g_{\tau R}g_{\mu L}^*g_{eL}g_{\mu R}^*\delta_{LR}^{\mu\tau}\delta_{RL}^{\mu e}\rvert$
$\tau^- \to \mu^-e^+\mu^+$	$44.6\{6.5\}[5.6\{0.8\}]$	$8.0\{9.2\}[1.0\{1.2\}]$	$11.3\{11.3\}[1.4\{1.4\}]$	$63.1\{31.5\}[7.9\{4.0\}]$

experimental values of Δa_e and Δa_μ. As Δa_e is generated from $Q_{\phi,\psi}\mathrm{Re}(g_{eR}^*g_{eL}\delta_{RL}^{ee})$, while Δa_μ is generated from $Q_{\phi,\psi}\mathrm{Re}(g_{\mu R}^*g_{\mu L}\delta_{RL}^{\mu\mu})$, the contributions are not from the same source (meaning the same ψ and ϕ). We also note that these values are larger than $Q_{\phi,\psi}\mathrm{Re}(g_{eR}^*g_{eL})$ and $Q_{\phi,\psi}\mathrm{Re}(g_{\mu R}^*g_{\mu L})$ in case I by roughly one order of magnitude. This is reasonable as we have cancellation in this case. Furthermore, comparing Figs. 3(b), 3(d), 8(a), and 8(b), we can clearly see the relaxation in the small-x region.

The upper limit in $\mu \to e\gamma$ decay gives the most severe constraints on photonic penguin contributions in $\mu \to e$ transitions, agreeing with [79,80], but the constraints on parameters are relaxed, especially in the small-x

region, comparing to case I. From Tables VIII–X and Figs. 9(a)–9(d), we see that the bounds on $\lvert Q_{\phi,\psi}g_{\mu R}^*g_{eR}\delta_{RR}^{\mu e}\rvert$ and $\lvert Q_{\phi,\psi}g_{\mu R}^*g_{eL}\delta_{RL}^{\mu e}\rvert$ are severely constrained by the $\mu \to e\gamma$ upper limit. Indeed, the $\mu \to e\gamma$ bound is more severe than the $\mu \to 3e$ and $\mu N \to eN$ bounds. The situation is altered when considering future experimental searches. From the tables and the figures, we see that, on the contrary, the $\mu \to 3e$ and $\mu N \to eN$ processes can probe the photonic penguin contributions from $\lvert Q_{\phi,\psi}g_{\mu R}^*g_{eR}\delta_{RR}^{\mu e}\rvert$ and $\lvert Q_{\phi,\psi}g_{\mu R}^*g_{eL}\delta_{RL}^{\mu e}\rvert$ better than the $\mu \to e\gamma$ decay in near future experiments.

Similar to case I, the Z-penguin diagrams can constrain chiral interaction better than photonic penguin diagrams in

TABLE X.   Same as Table VIII, but with $x \equiv m_\phi/m_\psi = 2$.

Processes	Constraints	Constraints	Constraints	Constraints
Δa_e	$Q_\phi\|g_{eR}\|^2$ -4234 ± 1732	$Q_\psi\|g_{eR}\|^2$ 3247 ∓ 1328	$Q_\phi\text{Re}(g_{eR}^*g_{eL}\delta_{RL}^{ee})$ $(13 \mp 6) \times 10^{-4}$	$Q_\psi\text{Re}(g_{eR}^*g_{eL}\delta_{RL}^{ee})$ $(-8 \pm 3) \times 10^{-4}$
Δa_μ	$Q_\phi\|g_{\mu R}\|^2$ 305 ± 82	$Q_\psi\|g_{\mu R}\|^2$ -234 ∓ 63	$Q_\phi\text{Re}(g_{\mu R}^*g_{\mu L}\delta_{RL}^{\mu\mu})$ $(-20 \mp 5) \times 10^{-3}$	$Q_\psi\text{Re}(g_{\mu R}^*g_{\mu L}\delta_{RL}^{\mu\mu})$ $(12 \pm 3) \times 10^{-3}$
Δa_τ	$Q_\phi\|g_{\tau R}\|^2$ $(-21 \sim 5) \times 10^6$	$Q_\psi\|g_{\tau R}\|^2$ $(-4 \sim 16) \times 10^6$	$Q_\phi\text{Re}(g_{\tau R}^*g_{\tau L}\delta_{RL}^{\tau\tau})$ $(-6 \sim 23) \times 10^3$	$Q_\psi\text{Re}(g_{\tau R}^*g_{\tau L}\delta_{RL}^{\tau\tau})$ $(-13 \sim 3) \times 10^3$
d_e, d_μ, d_τ	$\|Q_\phi\text{Im}(g_{eR}^*g_{eL}\delta_{RL}^{ee})\|$ 8.7×10^{-10}	$\|Q_\phi\text{Im}(g_{eR}^*g_{eL})\delta_{RL}^{ee}\|$ 5.0×10^{-10}	$\|Q_\phi\text{Im}(g_{lR}^*g_{lL}\delta_{RL}^{ll})\|_{l=\mu(\tau)}$ $15.0(126.2)$	$\|Q_\psi\text{Im}(g_{lR}^*g_{lL}\delta_{RL}^{ll})\|_{l=\mu(\tau)}$ $8.7(73.0)$
	$\|Q_\phi g_{\mu R}^* g_{eR}\delta_{RR}^{\mu e}\|$	$\|Q_\psi g_{\mu R}^* g_{eR}\delta_{RR}^{\mu e}\|$	$\|Q_\phi g_{\mu R}^* g_{eL}\delta_{RL}^{\mu e}\|$	$\|Q_\psi g_{\mu R}^* g_{eL}\delta_{RL}^{\mu e}\|$
$\mu^+ \to e^+\gamma$	$0.007[0.0027]$	$0.007[0.0027]$	$38[14] \times 10^{-8}$	$22[8] \times 10^{-8}$
$\mu^+ \to e^-e^+e^-$	$0.152[0.0015]$	$0.103[0.0010]$	$739[7] \times 10^{-8}$	$427[4] \times 10^{-8}$
$\mu^-\text{Au} \to e^-\text{Au}$	$0.069[0.0008]$	$0.064[0.0008]$	$777[9] \times 10^{-8}$	$449[5] \times 10^{-8}$
$\mu^-\text{Ti} \to e^-\text{Ti}$	$0.177[0.0003]$	$0.183[0.0003]$	$1875[3] \times 10^{-8}$	$1084[2] \times 10^{-8}$
$\mu^-\text{Al} \to e^-\text{Al}$	$[0.0003]$	$[0.0004]$	$[4 \times 10^{-8}]$	$[2 \times 10^{-8}]$
	$\|g_{\mu R}^* g_{eR}\Delta T_{3\psi}\delta_{RR}^{\mu e}\|$	$\|g_{\mu R}^* g_{eR}g_{eR}^* g_{eR}\delta_{RR}^{\mu e}\|$	$\|g_{\mu R}^* g_{eR}g_{eL}^* g_{eL}\delta_{RR}^{\mu e}\|$	
$\mu^+ \to e^-e^+e^-$	$142[1] \times 10^{-5}$	$0.07\{0.54\}[7\{54\} \times 10^{-4}]$	$0.12\{0.76\}[1\{8\} \times 10^{-3}]$	
$\mu^-\text{Au} \to e^-\text{Au}$	$178[2] \times 10^{-6}$			
$\mu^-\text{Ti} \to e^-\text{Ti}$	$623[1] \times 10^{-6}$			
$\mu^-\text{Al} \to e^-\text{Al}$	$[1 \times 10^{-6}]$			
	$\|Q_\phi g_{\tau R}g_{eR}^*\delta_{RR}^{e\tau}\|$	$\|Q_\psi g_{\tau R}g_{eR}^*\delta_{RR}^{e\tau}\|$	$\|Q_\phi g_{\tau R}g_{eL}^*\delta_{LR}^{e\tau}\|$	$\|Q_\psi g_{\tau R}g_{eL}^*\delta_{LR}^{e\tau}\|$
$\tau^- \to e^-\gamma$	$4.8[1.4]$	$4.7[1.4]$	$4.2[1.3] \times 10^{-3}$	$24[7] \times 10^{-4}$
$\tau^- \to e^-e^+e^-$	$43.7[5.5]$	$33.9[4.3]$	$37[5] \times 10^{-3}$	$21[3] \times 10^{-3}$
	$\|g_{\tau R}g_{eR}^*\Delta T_{3\psi}\delta_{RR}^{e\tau}\|$	$\|g_{\tau R}g_{eR}^*g_{eR}g_{eR}^*\delta_{RR}^{e\tau}\|$	$\|g_{\tau R}g_{eR}^*g_{eL}g_{eL}^*\delta_{RR}^{e\tau}\|$	
$\tau^- \to e^-e^+e^-$	$0.56[0.07]$	$28.3\{210.5\}[3.6\{26.6\}]$	$46.3\{297.7\}[5.8\{37.6\}]$	
	$\|Q_\phi g_{\tau R}g_{\mu R}^*\delta_{RR}^{\mu\tau}\|$	$\|Q_\psi g_{\tau R}g_{\mu R}^*\delta_{RR}^{\mu\tau}\|$	$\|Q_\phi g_{\tau R}g_{\mu L}^*\delta_{LR}^{\mu\tau}\|$	$\|Q_\psi g_{\tau R}g_{\mu R}^*\delta_{LR}^{\mu\tau}\|$
$\tau^- \to \mu^-\gamma$	$5.5[0.8]$	$5.4[0.8]$	$49[7] \times 10^{-4}$	$28[4] \times 10^{-4}$
$\tau^- \to \mu^-\mu^+\mu^-$	$38.5[4.8]$	$29.9[3.7]$	$33[4] \times 10^{-3}$	$19[2] \times 10^{-3}$
	$\|g_{\tau R}g_{\mu R}^*\Delta T_{3\psi}\delta_{RR}^{\mu\tau}\|$	$\|g_{\tau R}g_{\mu R}^*g_{\mu R}g_{\mu R}^*\delta_{RR}^{\mu\tau}\|$	$\|g_{\tau R}g_{\mu R}^*g_{\mu L}g_{\mu L}^*\delta_{RR}^{\mu\tau}\|$	
$\tau^- \to \mu^-\mu^+\mu^-$	$0.49[0.06]$	$25.0\{185.6\}[3.1\{23.3\}]$	$40.9\{262.5\}[5.1\{32.9\}]$	
	$\|g_{\tau R}g_{eR}^*g_{\mu R}g_{eR}^*\delta_{RR}^{e\tau}\delta_{RR}^{e\mu}\|$	$\|g_{\tau R}g_{eR}^*g_{\mu L}g_{eL}^*\delta_{RR}^{e\tau}\delta_{LL}^{e\mu}\|$	$\|g_{\tau R}g_{eL}^*g_{\mu R}g_{eL}^*\delta_{LR}^{e\tau}\delta_{LR}^{e\mu}\|$	$\|g_{\tau R}g_{eL}^*g_{\mu L}g_{eR}^*\delta_{LR}^{e\tau}\delta_{RL}^{e\mu}\|$
$\tau^- \to e^-\mu^+e^-$	$41.9\{194.1\}[5.3\{24.5\}]$	$48.7\{274.5\}[6.2\{34.7\}]$	$68.9\{68.9\}[8.7\{8.7\}]$	$59.3\{29.6\}[7.5\{3.7\}]$
	$\|g_{\tau R}g_{\mu R}^*g_{eR}g_{\mu R}^*\delta_{RR}^{\mu\tau}\delta_{RR}^{\mu e}\|$	$\|g_{\tau R}g_{\mu R}^*g_{eL}g_{\mu L}^*\delta_{RR}^{\mu\tau}\delta_{LL}^{\mu e}\|$	$\|g_{\tau R}g_{\mu L}^*g_{eR}g_{\mu L}^*\delta_{LR}^{\mu\tau}\delta_{LR}^{\mu e}\|$	$\|g_{\tau R}g_{\mu L}^*g_{eL}g_{\mu R}^*\delta_{LR}^{\mu\tau}\delta_{RL}^{\mu e}\|$
$\tau^- \to \mu^-e^+\mu^+$	$44.6\{206.6\}[5.6\{26.0\}]$	$51.9\{292.2\}[6.5\{36.8\}]$	$73.4\{73.4\}[9.2\{9.4\}]$	$63.1\{31.5\}[7.9\{4.0\}]$

FIG. 8.   Allowed parameter space for (a) $\pm Q_{\phi,\psi}\text{Re}(g_{eR}^*g_{eL}\delta_{RL}^{ee})$ and $Q_{\phi,\psi}\text{Im}(g_{eR}^*g_{eL}\delta_{RL}^{ee})|$ constrained by Δa_μ and d_e, respectively, and (b) $\mp Q_{\phi,\psi}\text{Re}(g_{\mu R}^*g_{\mu L}\delta_{RL}^{\mu\mu})$ and $Q_{\phi,\psi}\text{Im}(g_{\mu R}^*g_{\mu L}\delta_{RL}^{\mu\mu})|$ constrained by Δa_μ and d_μ, respectively. These constrains are obtained using $m_\psi = 500$ GeV, for other m_ψ, apply $(100 \text{ GeV})/m_\psi$ to the plots.
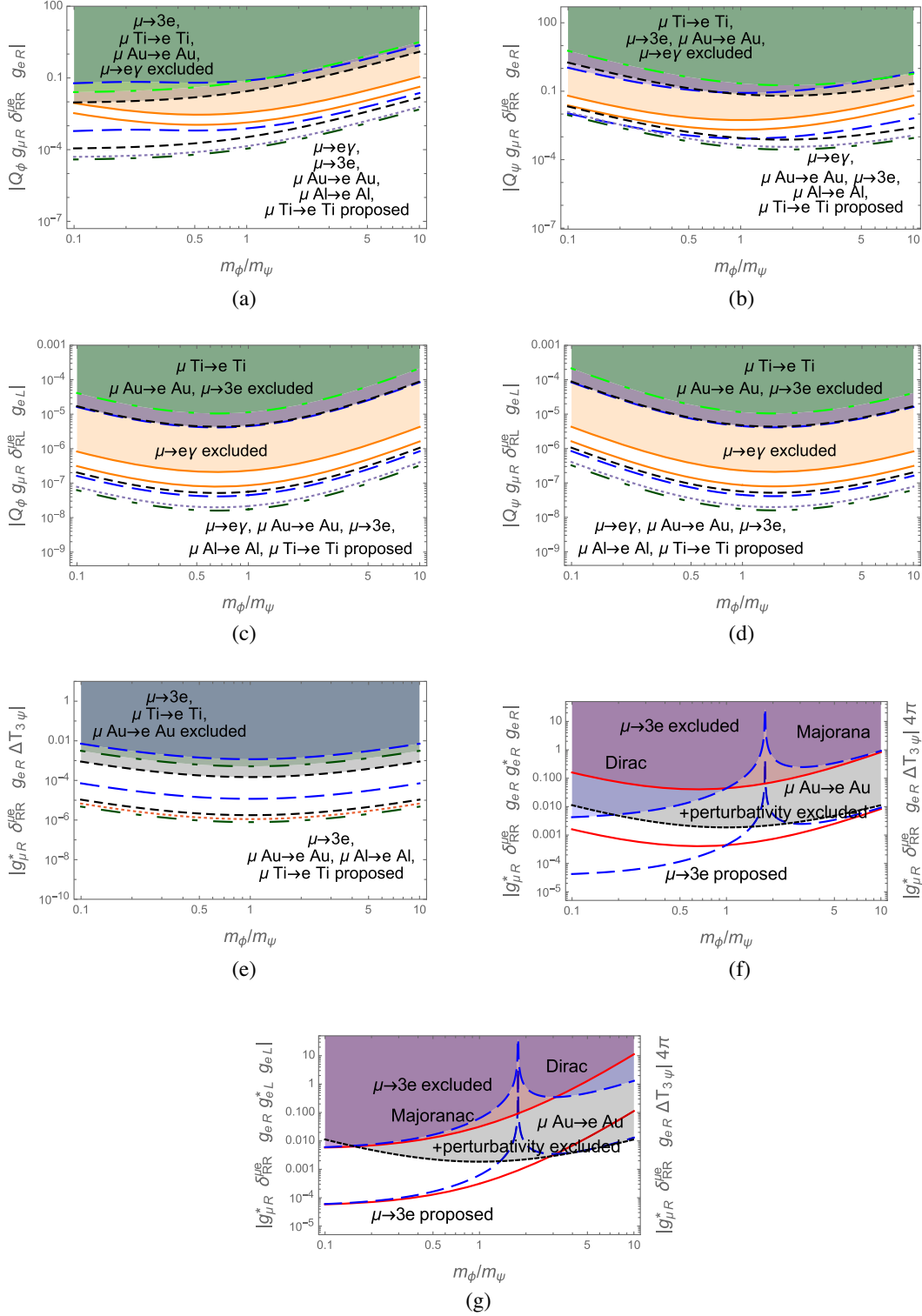
FIG. 9.   Same as Fig. 4, but for case II.

$\mu \to e$ transitions. From Tables VIII–X, Figs. 9(a), 9(b), and 9(e) we see that the bounds on $|g_{\mu R}^* g_{eR} \Delta T_{3\psi} \delta_{RR}^{\mu e}|$ from Z-penguin contributions are more severe (by one to two orders of magnitude) than the bounds on $|Q_{\phi,\psi} g_{\mu R}^* g_{eR} \delta_{RR}^{\mu e}|$ from photonic penguin contributions. In addition, from

Fig. 9(e) we see that the upper limits of $\mu N \to eN$ transitions give better bounds on $|g_{\mu R}^* g_{eR} \Delta T_{3\psi} \delta_{RR}^{\mu e}|$ than the $\mu \to 3e$ bound.

For x larger than 0.2, box contributions to $\mu \to 3e$ decay are subleading comparing to Z penguin contributions,
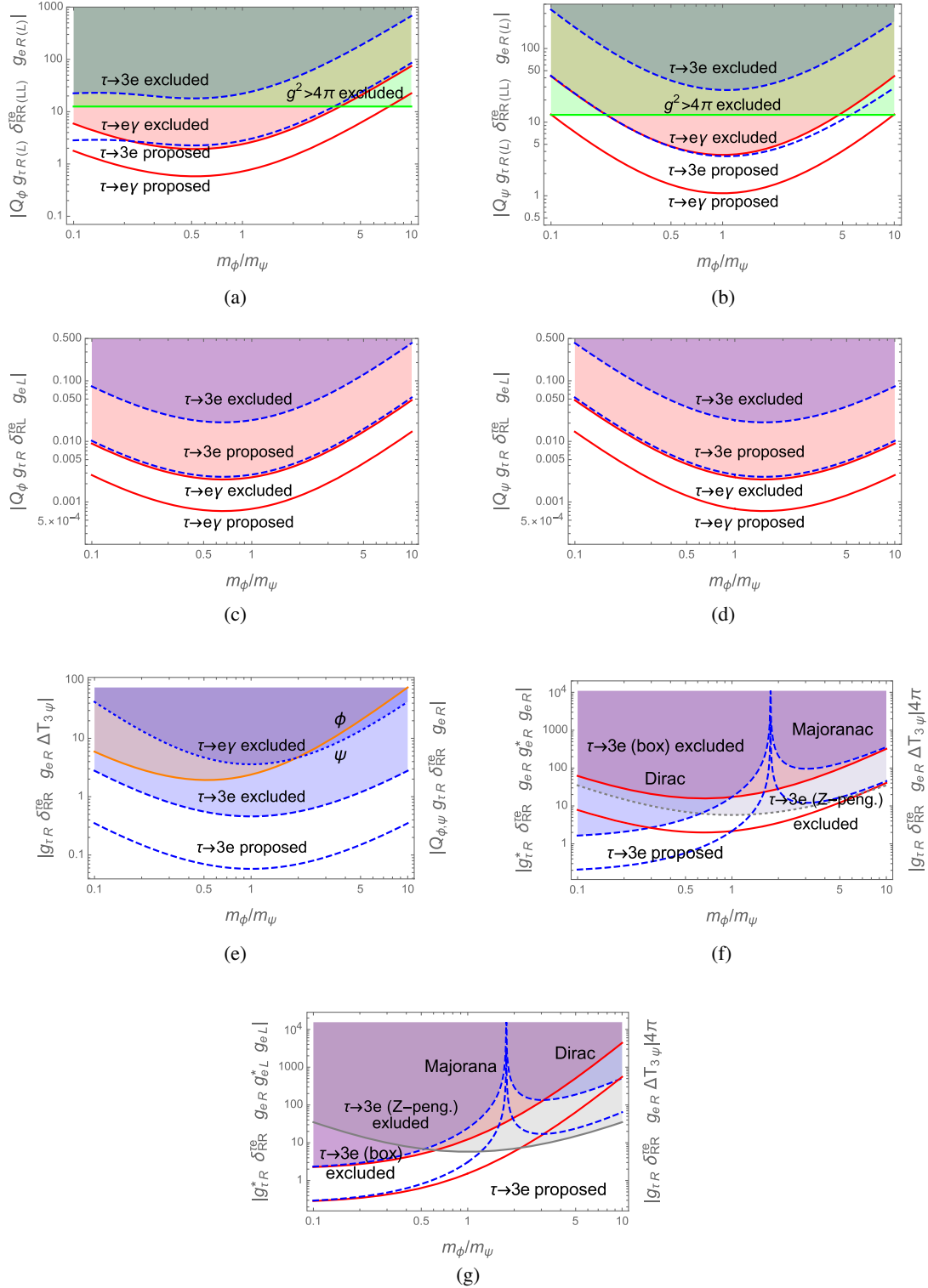
FIG. 10. Same as Fig. 5, but for case II.

but the former can be important for $x \lesssim 0.2$. In Figs. 9(f) and 9(g) we show the bounds on $|g_{\mu R}^* g_{eR} \delta_{RR}^{\mu e} g_{eR}^* g_{eR}|$ and $|g_{\mu R}^* g_{eR} \delta_{RR}^{\mu e} g_{eL}^* g_{eL}|$ obtained by considering box contributions to $\mu \to 3e$ decay. Note that the constraint on $|g_{\mu R}^* g_{eR} \Delta T_{3\psi} \delta_{RR}^{\mu e}||g_{eR(L)}^* g_{eR(L)}|$ obtained from $\mu Au \to eAu$ upper limit and perturbativity is much severe than the $|g_{\mu R}^* \delta_{RR}^{\mu e} g_{eR} g_{eR(L)}^* g_{eR(L)}|$ bound. However for x smaller than 0.2, box contributions can be important. This is different from case I, as penguin contributions have larger cancellation in the small-x region in the present case and, as
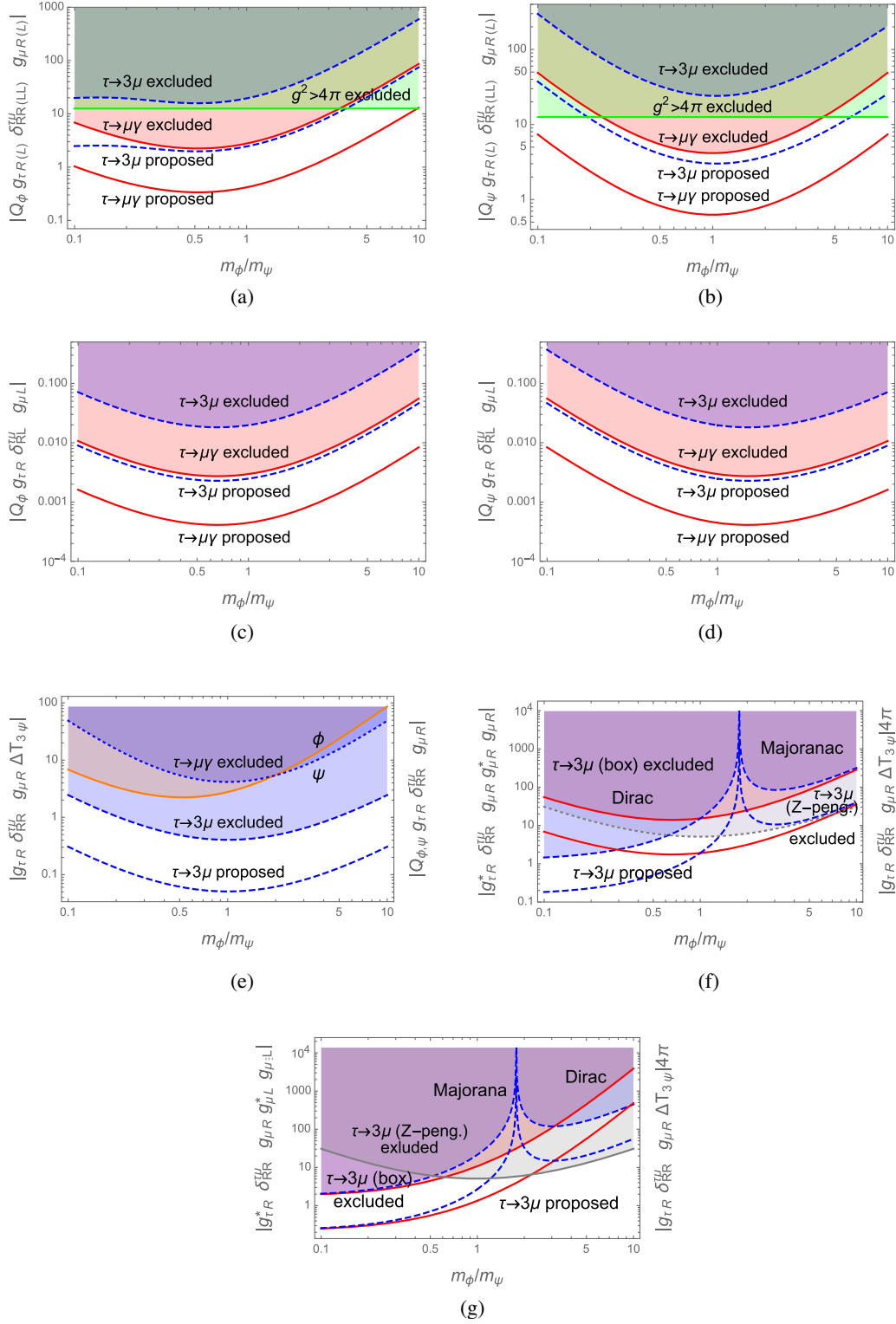
FIG. 11. Same as Fig. 6, but for case II.

a result, box contributions become relatively important in this region.

From Tables VIII–X, we see that similar to case I the present bound on Δa_τ cannot constrain $Q_{\phi,\psi}|g_{\tau R(L)}|^2$ and

$Q_{\phi,\psi}\mathrm{Re}(g^*_{\tau R}g_{\tau L}\delta^{\tau\tau}_{RL})$ well. Even the bound on d_τ cannot give good constraints on $Q_{\phi,\psi}\mathrm{Im}(g^*_{\tau R}g_{\tau L}\delta^{\tau\tau}_{RL})$.

In $\tau \to e \ (\mu)$ transitions, the $\tau \to e\gamma(\mu\gamma)$ upper limit constrains photonic penguin contributions better than
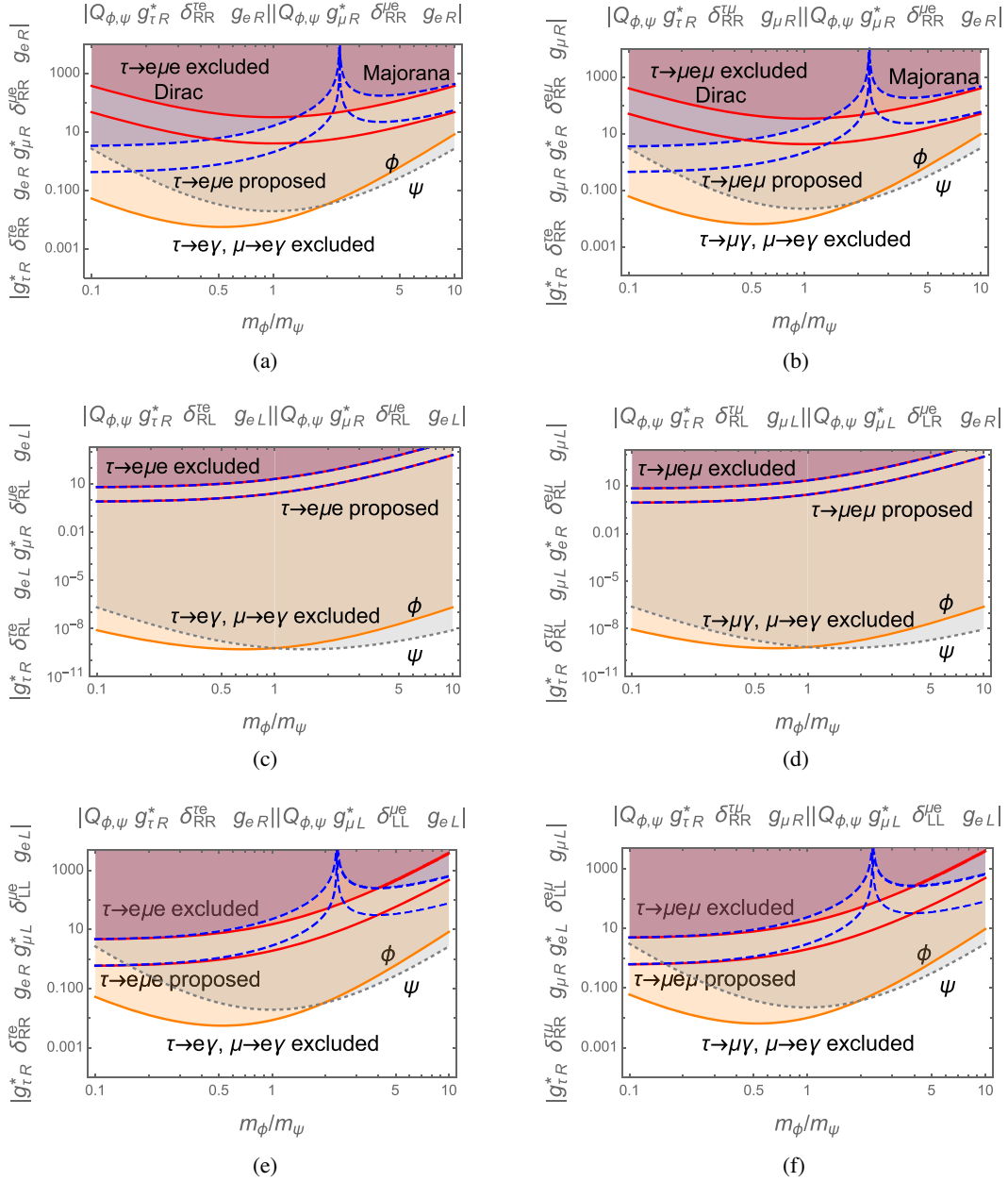
FIG. 12. Same as Fig. 7, but for case II.

the $\tau \to 3e \ (3\mu)$ upper limit, agreeing with [80], and the Z-penguin constrains chiral interaction better than the photonic penguin. From Tables VIII–X, Figs. 10(a)–10(d) and 11(a)–11(d), we see that bounds on $|Q_{\phi,\psi} g_{\tau R}^* g_{e(\mu)R} \delta_{RR}^{\tau e(\tau\mu)}|$ and $|Q_{\phi,\psi} g_{\tau R}^* g_{e(\mu)L} \delta_{RL}^{\tau e(\tau\mu)}|$ are constrained by the $\tau \to e\gamma (\mu\gamma)$ data more severely than by the $\tau \to 3e \ (3\mu)$ upper limit. Note that even the bounds using the proposed sensitivities on $\tau \to 3e$ and $\tau \to 3\mu$ decays in Belle II are superseded by the bounds using the present limits of $\tau \to e\gamma$ and $\tau \to \mu\gamma$ decays in most of the parameter space. From Tables VIII–X, Figs. 10(e) and 11(e), we see that bounds on $|g_{\tau R}^* g_{e(\mu)R} \Delta T_{3\psi} \delta_{RR}^{\tau e(\tau\mu)}|$

from Z-penguin contributions are more severe (by one order of magnitude) than those on $|Q_{\phi,\psi} g_{\tau R}^* g_{e(\mu)R}|$ from photonic penguin contributions. Hence, Z-penguin constrains chiral interaction better than photonic penguin. These features are similar to case I, but comparing Figs. 5, 6, 10, and 11 we can clearly see that the bounds are significant relaxed in the small-x region in the present case.

Box contributions to $\tau \to 3e$ and $\tau \to 3\mu$ decays can sometime be comparable to Z-penguin contributions. We show in Figs. 10(g), 10(h), 11(g), and 11(h) the bounds on $|g_{\tau R}^* g_{e(\mu)R} \delta_{RR}^{\tau e(\tau\mu)} g_{e(\mu)R}^* g_{e(\mu)R}|$ and $|g_{\tau R}^* g_{e(\mu)R} \delta_{RR}^{\tau e(\tau\mu)} g_{e(\mu)L}^* g_{e(\mu)L}|$ obtained by considering box contributions to $\tau \to 3e \ (3\mu)$

TABLE XI. Same as Table VII, but for case II.

	Current limit (future sensitivity)	Consistency bounds	Remarks
$\mathcal{B}(\mu^+ \to e^+\gamma)$	$<4.2 \times 10^{-13}$ (6×10^{-14})	$<4.2 \times 10^{-13}$	Input
$\mathcal{B}(\mu^+ \to e^+e^+e^-)$	$<1.0 \times 10^{-12}$ (10^{-16})	$<2.2 \times 10^{-14}$	From $\mu \to e\gamma$ bound
		$<1.6 \times 10^{-14}$	From $\mu\text{Au} \to e\text{Au}$ bound
$\mathcal{B}(\mu^-\text{Ti} \to e^-\text{Ti})$	$<4.3 \times 10^{-12}$ (10^{-17})	$<5.2 \times 10^{-14}$	From $\mu \to e\gamma$ bound
		$<3.5 \times 10^{-13}$	From $\mu\text{Au} \to e\text{Au}$ bound
$\mathcal{B}(\mu^-\text{Au} \to e^-\text{Au})$	$<7.0 \times 10^{-13}$ (10^{-16})	$<6.2 \times 10^{-13}$	From $\mu \to e\gamma$ bound
		$<7.0 \times 10^{-13}$	Input
$\mathcal{B}(\mu^-\text{Al} \to e^-\text{Al})$	$\cdots$ (10^{-17})	$<3.2 \times 10^{-13}$	From $\mu \to e\gamma$ bound
		$<1.7 \times 10^{-13}$	From $\mu\text{Au} \to e\text{Au}$ bound
$\mathcal{B}(\tau^- \to e^-\gamma)$	$<3.3 \times 10^{-8}$ (3×10^{-9})	$<3.3 \times 10^{-8}$	Input
$\mathcal{B}(\tau^- \to e^-e^+e^-)$	$<2.7 \times 10^{-8}$ (4.3×10^{-10})	$<1.9 \times 10^{-9}$	From $\tau \to e\gamma$ bound
$\mathcal{B}(\tau^- \to \mu^-\gamma)$	$<4.4 \times 10^{-8}$ (1×10^{-9})	$<4.4 \times 10^{-8}$	Input
$\mathcal{B}(\tau^- \to \mu^-\mu^+\mu^-)$	$<2.1 \times 10^{-8}$ (3.3×10^{-10})	$<2.5 \times 10^{-9}$	From $\tau \to \mu\gamma$ bound
$\mathcal{B}(\tau^- \to \mu^-e^+\mu^-)$	$<1.7 \times 10^{-8}$ (2.7×10^{-10})	$\lesssim 1.3 \times 10^{-8}$	From $\tau \to \mu\gamma, \mu \to e\gamma$ bounds
$\mathcal{B}(\tau^- \to e^-\mu^+e^-)$	$<1.5 \times 10^{-8}$ (2.4×10^{-10})	$\lesssim 1 \times 10^{-8}$	From $\tau \to e\gamma, \mu \to e\gamma$ bounds

decay. Note that the constraint on $|g_{\tau R}^* g_{e(\mu)R} \delta_{RR}^{\tau e(\tau\mu)} \Delta T_{3\psi}| \times |g_{e(\mu)L}^* g_{e(\mu)L}|$ obtained from Z-penguin contributions to $\tau \to 3e \, (3\mu)$ decay and perturbativity is much severe than the $|g_{\tau R}^* g_{e(\mu)R} \delta_{RR}^{\tau e(\tau\mu)} g_{e(\mu)R}^* g_{e(\mu)R}|$ bound for $x \gtrsim 0.6$, but it is the other way around for $x \lesssim 0.6$. One can also obtain these results using the values in Tables VIII–X. These results imply that box contributions to $\tau \to 3e, 3\mu$ can sometime be comparable to Z-penguin contributions. This is similar to case I, but in a different region of x.

The $\tau^- \to e^-\mu^+e^-$ rate is constrained by $\tau \to e\gamma$ and $\mu \to e\gamma$ upper limits. The bounds on $|g_{\tau R}^* g_{eR} \delta_{RR}^{\tau e} g_{\mu R}^* g_{eR} \delta_{RR}^{\mu e}|$, $|g_{\tau R}^* g_{eL} \delta_{RL}^{\tau e} g_{\mu R}^* g_{eL} \delta_{RL}^{\tau e}|$, and $|g_{\tau R}^* g_{eR} \delta_{RR}^{\tau e} g_{\mu L}^* g_{eL} \delta_{LL}^{\mu e}|$ obtained from constraining box contributions using the upper limit of the $\tau^- \to e^-\mu^+e^-$ rate are shown in Figs. 12(a), 12(c), and 12(e), Tables VIII–X. They are larger than the bounds on $|Q_{\phi,\psi} g_{\tau R}^* g_{eR} \delta_{RR}^{\tau e}||Q_{\phi,\psi} g_{\mu R}^* g_{eR} \delta_{RR}^{\mu e}|$, $|Q_{\phi,\psi} g_{\tau R}^* g_{eL} \delta_{RL}^{\tau e}| \times |Q_{\phi,\psi} g_{\mu R}^* g_{eL} \delta_{RL}^{\mu e}|$, and $|Q_{\phi,\psi} g_{\tau R}^* g_{eR} \delta_{RR}^{\tau e}||Q_{\phi,\psi} g_{\mu L}^* g_{eL} \delta_{LL}^{\mu e}|$ obtained by using the upper limits of $\tau \to e\gamma$ and $\mu \to e\gamma$ rates. Note that for $x \gtrsim 0.2$ even the proposed sensitivity on $\tau^- \to e^-\mu^+e^-$ rate is constrained. Hence, the $\tau^- \to e^-\mu^+e^-$ rate is constrained by the present $\tau \to e\gamma$ and $\mu \to e\gamma$ upper limits. This is similar to case I, but the constraints from $\tau \to e\gamma$ and $\mu \to e\gamma$ upper limits are relatively relaxed.

Similarly the $\tau^- \to \mu^-e^+\mu^-$ rate is constrained by $\tau \to \mu\gamma$ and $\mu \to e\gamma$ upper limits. From Figs. 12(b), 12(d), and 12(f), Tables VIII–X, we see that the bounds on $|g_{\tau R}^* g_{\mu R} \delta_{RR}^{\tau\mu} g_{eR}^* g_{\mu R} \delta_{RR}^{e\mu}|$, $|g_{\tau R}^* g_{\mu L} \delta_{RL}^{\tau\mu} g_{eR}^* g_{\mu L} \delta_{RL}^{e\mu}|$, and $|g_{\tau R}^* g_{\mu R} \delta_{RR}^{\tau\mu} g_{eL}^* g_{\mu L} \delta_{RR}^{e\mu}|$ obtained from the upper limit of the $\tau^- \to \mu^-e^+\mu^-$ rate are larger than the bounds on $|Q_{\phi,\psi} g_{\tau R}^* g_{\mu R} \delta_{RR}^{\tau\mu}||Q_{\phi,\psi} g_{\mu R}^* g_{eR} \delta_{RR}^{\mu e}|$, $|Q_{\phi,\psi} g_{\tau R}^* g_{\mu L} \delta_{RL}^{\tau\mu}| \times |Q_{\phi,\psi} g_{\mu L}^* g_{eR} \delta_{LR}^{\mu e}|$, and $|Q_{\phi,\psi} g_{\tau R}^* g_{\mu R} \delta_{RR}^{\tau\mu}||Q_{\phi,\psi} g_{\mu L}^* g_{eL} \delta_{LL}^{\mu e}|$ obtained from the upper limits of $\tau \to \mu\gamma$ and $\mu \to e\gamma$

rates. Hence, the $\tau^- \to \mu^-e^+\mu^-$ rate is constrained by $\tau \to \mu\gamma$ and $\mu \to e\gamma$ upper limits. Note that for $x \gtrsim 0.2$ even the proposed sensitivity on $\tau^- \to \mu^-e^+\mu^-$ rate is highly constrained. This is similar to case I, but the constraints obtained using $\tau \to \mu\gamma$ and $\mu \to e\gamma$ upper limits are relatively relaxed.

In Table XI, we compare the current experimental upper limits, future sensitivities, and bounds from consistency for case II on various muon and tau LFV processes. We see that the present $\mu \to e\gamma$ upper limit requires the bounds on $\mu \to 3e$ and $\mu\text{Ti} \to e\text{Ti}$ be lower by more than one order of magnitude from their present upper limits, while the $\mu\text{Au} \to e\text{Au}$ bound is close to its present limit and the $\mu\text{Al} \to e\text{Al}$ rate is predicted to be smaller than 3×10^{-13}. Comparing to case I we see that the $\mu \to 3e$, $\mu\text{Au} \to e\text{Au}$, and $\mu\text{Al} \to e\text{Al}$ bounds are relaxed, while the $\mu\text{Ti} \to e\text{Ti}$ bound is tighten. We find that the situation is similar when the present $\mu\text{Au} \to e\text{Au}$ upper limit instead of the present $\mu \to e\gamma$ upper limit is used as an input. Using the present $\tau \to e\gamma(\mu\gamma)$ upper limit as input, the $\tau \to 3e \, (3\mu)$ bound is smaller than its present upper limit by one order of magnitude. These bounds are relaxed compared to those in case I. Note that the $\mathcal{B}(l' \to l\bar{l}l)/\mathcal{B}(l' \to l\gamma)$ ratios are close to the values shown in Eq. (8) [79,80], but not identical to them, as the F_1 terms in photonic penguins also play some roles. Finally, the $\tau^- \to \mu^-e^+\mu^-$ and $\tau^- \to e^-\mu^+e^-$ bounds are similar to their present upper limits when the present $\tau \to \mu\gamma$, $e\gamma$ and $\mu \to e\gamma$ upper limits are used. These limits are significantly relaxed compared to those in case I.

IV. CONCLUSION

We study anomalous magnetic moments and lepton flavor violating processes of e, μ, and τ leptons in this work. We use a data driven approach to investigate the

implications of the present data on the parameters of a class of models, which has spin-0 scalar and spin-1/2 fermion fields and can contribute to Δa_l and LFV processes. We compare two different cases, case I and case II, which does not have and has a built-in cancelation mechanism, respectively. Our findings are as follows.

(i) Parameters are constrained using the present data of Δa_l, d_l and lepton flavor violating processes of e, μ and τ leptons.

(ii) The built-in cancelation has more prominent effects in penguin amplitudes than in box amplitudes. Furthermore, the cancelation affects amplitudes in small-x ($x \equiv m_\phi/m_\psi$) region more effectively.

(iii) Chiral interactions are unable to generate large enough Δa_e and Δa_μ to accommodate the experimental results.

(iv) Although Δa_e and Δa_μ can be successfully generated to accommodate the experimental results by using nonchiral interactions, they are not contributed from the same source. This agrees with the finding in [27].

(v) Presently, the upper limit in $\mu \to e\gamma$ decay gives the most severe constraints on photonic penguin contributions in $\mu \to e$ transitions, agreeing with [79,80], but the situation may change in considering future experimental sensitivities. In fact, the future $\mu \to 3e$ and $\mu N \to eN$ experiments may probe the photonic penguin contributions better than the future $\mu \to e\gamma$ experiment.

(vi) The Z-penguin diagrams can constrain chiral interaction better than photonic penguin diagrams in $\mu \to e$ transitions. In addition, $\mu N \to eN$ transitions constrain Z-penguin contributions better $\mu \to 3e$ decay.

(vii) In case I, either in the Dirac or Majorana case, box contributions to $\mu \to 3e$ decay are subleading. Furthermore, there are cancelation in box contributions in the Majorana fermionic case making the contributions even smaller. In case II, we find that for $x \gtrsim 0.2$, box contributions to $\mu \to 3e$ decay are subleading comparing to Z penguin contributions, but they can be important for $x \lesssim 0.2$.

(viii) The present bounds on Δa_τ and d_τ are unable to give useful constraints on parameters.

(ix) In $\tau \to e$ (μ) transitions, the $\tau \to e\gamma(\mu\gamma)$ upper limit constrains photonic penguin contributions better than the $\tau \to 3e$ (3μ) upper limit, agreeing with [80], and Z-penguin constrains chiral interaction better than photonic penguin. Note that even the bounds using the proposed sensitivities on $\tau \to 3e$ and $\tau \to 3\mu$ decays by Belle II are superseded by the bounds using the present limits of $\tau \to e\gamma$ and $\tau \to \mu\gamma$ decays for most of the parameter space. Bounds are significantly relaxed in the small-x region in case II.

(x) Box contributions to $\tau \to 3e$ and $\tau \to 3\mu$ decays can sometime be comparable to Z-penguin contributions.

(xi) The $\tau^- \to e^-\mu^+e^-$ rate is highly constrained by $\tau \to e\gamma$ and $\mu \to e\gamma$ upper limits. Note that in case I even the proposed sensitivity on $\tau^- \to e^-\mu^+e^-$ rate is highly constrained, but in case II, for $x \lesssim 0.2$ the constraints are relaxed.

(xii) The $\tau^- \to \mu^-e^+\mu^-$ rate is also highly constrained by $\tau \to \mu\gamma$ and $\mu \to e\gamma$ upper limits. Note that in case I even the proposed sensitivity on $\tau^- \to \mu^-e^+\mu^-$ rate is highly constrained, but in case II, for $x \lesssim 0.2$ the constraints are relaxed.

(xiii) We compare the current experimental upper limits, future sensitivities and bounds from consistency on various muon and tau LFV processes:

(a) In case I, the present $\mu \to e\gamma$ upper limit requires the bounds on $\mu \to 3e$, $\mu\text{Ti} \to e\text{Ti}$ and $\mu\text{Au} \to e\text{Au}$ be lower by two orders of magnitude, more than one order of magnitude and almost one order of magnitude, respectively, from their present upper limits, and the $\mu\text{Al} \to e\text{Al}$ rate is predicted to be smaller than 6×10^{-14}. In case II, the $\mu \to 3e$, $\mu\text{Au} \to e\text{Au}$ and $\mu\text{Al} \to e\text{Al}$ bounds are relaxed, while the $\mu\text{Ti} \to e\text{Ti}$ bound is tighten. We agree with [80] that presently the $\mathcal{B}(\mu \to e\gamma)$ upper limit provides the most severe constrain on NP contributing to $\mu \to e$ transitions.

(b) We find that the situation is similar but the bounds are slightly relaxed when the $\mu\text{Au} \to e\text{Au}$ upper limit instead of the present $\mu \to e\gamma$ upper limit is used as an input.

(c) Using the present $\tau \to e\gamma(\mu\gamma)$ upper limit as input, the $\tau \to 3e$ (3μ) bound is smaller than its present upper limit by one order of magnitude.

(d) In case I, the $\tau^- \to \mu^-e^+\mu^-$ and $\tau^- \to e^-\mu^+e^-$ bounds are lower than their present upper limits by two orders of magnitude as required from the present $\tau \to \mu\gamma$, $e\gamma$ and $\mu \to e\gamma$ upper limits. These limits are lower than the proposed future sensitivities. In case II, the $\tau^- \to \mu^-e^+\mu^-$ and $\tau^- \to e^-\mu^+e^-$ bounds are similar to their present upper limits when the present $\tau \to \mu\gamma$, $e\gamma$ and $\mu \to e\gamma$ upper limits are used. These limits are significant relaxed compared to those in case I.

ACKNOWLEDGMENTS

APPENDIX A: FORMULAS FOR VARIOUS PROCESSES

Formulas in this Appendix are taken from Ref. [82] and are updated. In the weak bases of ψ_{Lp}, ψ_{Rp}, ϕ_{La}, and ϕ_{Ra}, the interacting Lagrangian is given by

$$\mathcal{L}_{int} = (g'^{pa}_{lL} \bar{\psi}_{Rp} l_L \phi^*_{La} + g'^{pa}_{lR} \bar{\psi}_{Lp} l_R \phi^*_{Ra}) + \text{H.c.}, \quad \text{(A1)}$$

where $\phi_{L(R)}$ are scalar fields coupling to $l_{L(R)}$ and p, a indicate weak quantum numbers. Fields in the weak bases can be transformed into those in the mass bases,

$$\phi_i = U^L_{ia} \phi_{La} + U^R_{ia} \phi_{Ra}, \qquad \psi_{nL(R)} = V^{L(R)}_{np} \psi_{L(R)p}, \quad \text{(A2)}$$

with the help of mixing matrices, U and V. It is useful to define

$$g^{ni}_{lL(R)} \equiv g'^{pa}_{lL(R)} V^{R(L)}_{np} U^{L(R)}_{ia} \quad \text{(A3)}$$

and, consequently, the interacting Lagrangian can be expressed as in Eq. (12).

The effective Lagrangian for various precesses is given by

$$\mathcal{L}_{\text{eff}} = \mathcal{L}_{l'l\gamma} + \mathcal{L}_{l'll''l} + \mathcal{L}_{l'lqq} \quad \text{(A4)}$$

with $l^{(',''}) = e, \mu, \tau$ denoting leptons and q denoting quarks. For $l' \neq l$, we have

$$\mathcal{L}_{l'l\gamma} = \bar{l}'_L \sigma_{\mu\nu} l_R F^{\mu\nu} A_{L'R} + \bar{l}'_R \sigma_{\mu\nu} l_L F^{\mu\nu} A_{R'L} + \text{H.c.}, \quad \text{(A5)}$$

and

$$A_{LR'} = A^*_{R'L}, \qquad A_{RL'} = A^*_{L'R}, \quad \text{(A6)}$$

while for $l' = l$, the additional Hermitian conjugated terms in Eq. (A5) are not required. These As are from

the so-called photonic dipole penguin. The relevant effective Lagrangians responsible for $\bar{l}' \to \bar{l} l'' \bar{l}$ decays and $l' \to l$ conversion processes are given by [19]

$$\begin{aligned}\mathcal{L}_{l'll''l} = &\, g_{RLRL}(\bar{l}'_R l_L)(\bar{l}''_R l_L) + g_{LRLR}(\bar{l}'_L l_R)(\bar{l}''_L l_R) \\ &+ g_{RRRR}(\bar{l}'_R \gamma^\mu l_R)(\bar{l}''_R \gamma_\mu l_R) + g_{LLLL}(\bar{l}'_L \gamma^\mu l_L)(\bar{l}''_L \gamma_\mu l_L) \\ &+ g_{RRLL}(\bar{l}'_R \gamma^\mu l_R)(\bar{l}''_L \gamma_\mu l_L) + g_{LLRR}(\bar{l}'_L \gamma^\mu l_L)(\bar{l}''_R \gamma_\mu l_R) \\ &+ \text{H.c.}, \end{aligned} \quad \text{(A7)}$$

$$\mathcal{L}_{l'lqq} = \sum_{q=u,d} [g_{LV}(q) \bar{l}'_L \gamma^\mu l_L + g_{RV}(q) \bar{l}'_R \gamma^\mu l_R] \bar{q} \gamma_\mu q + \text{H.c.}, \quad \text{(A8)}$$

where

$$\begin{aligned}g_{MNOP} &\equiv e^2 Q_l g^\gamma_{M'M} \delta_{MN} \delta_{OP} \delta_{ll''} + g^Z_{M'M} g^Z_{l_O} \delta_{MN} \delta_{OP} \delta_{ll''} \\ &\quad + g^B_{MNOP}, \end{aligned}$$

$$g_{M'V}(q) \equiv e^2 Q_q g^\gamma_{M'M} + \frac{1}{2} g^Z_{M'M}(g^Z_{q_L} + g^Z_{q_R}),$$

$$g^Z_X \equiv \frac{e}{\sin\theta_W \cos\theta_W}(T_3 - \sin^2\theta_W Q)_X, \quad \text{(A9)}$$

with $M, N, O, P = L, R$, $g^\gamma_{M'M}$ from the nonphotonic dipole penguin, $g^Z_{M'M}$ from the Z-penguin, g^B_{MNOP} from the box diagrams and $X = l_L, l_R, q_L, q_R$ and so on.

Using Eq. (12), the Wilson coefficients for $\mathcal{L}_{l'l\gamma}$ in Eq. (A5) can be calculated to be [82]

$$\begin{aligned}A_{M'N} = \frac{e}{32\pi^2} &[(m_{l'} g^{ni*}_{l'N} g^{ni}_{lN} + m_l g^{ni*}_{l'M} g^{ni}_{lM})(Q_{\phi_i} F_1(m^2_{\psi_n}, m^2_{\phi_i}) - Q_{\psi_n} F_1(m^2_{\phi_i}, m^2_{\psi_n})) \\ &+ m_{\psi_n} g^{ni*}_{l'M} g^{ni}_{lN}(Q_{\phi_i} F_3(m^2_{\psi_n}, m^2_{\phi_i}) - Q_{\psi_n} F_2(m^2_{\phi_i}, m^2_{\psi_n}))], \end{aligned} \quad \text{(A10)}$$

for M different from N, and F_i are loop functions with the explicit forms to be given below. The Wilson coefficients for $\mathcal{L}_{l'll''l}$ and $\mathcal{L}_{l'lqq}$ in Eq. (A9) are given by

$$\begin{aligned}g^\gamma_{R'R} &= \frac{1}{16\pi^2} \{ g^{ni*}_{l'R} g^{ni}_{lR}[Q_{\psi_n} G_2(m^2_{\phi_i}, m^2_{\psi_n}) + Q_{\phi_i} G_1(m^2_{\psi_n}, m^2_{\phi_i})] \\ &\quad + m_{\psi_n}(m_{l'} g^{ni*}_{l'L} g^{ni}_{lR} + m_l g^{ni*}_{l'R} g^{ni}_{lL})[Q_{\psi_n} G_3(m^2_{\phi_i}, m^2_{\psi_n}) + Q_{\phi_i} G_3(m^2_{\psi_n}, m^2_{\phi_i})] \} \\ g^Z_{R'R} &= -\frac{e}{16\pi^2 m^2_Z \sin 2\theta_W} 2\kappa_{Rijmn} g^{mi*}_{l'R} g^{nj}_{lR} F_Z(m^2_{\psi_m}, m^2_{\psi_n}, m^2_{\phi_i}, m^2_{\phi_j}, m^2_Z) \\ &\quad - \frac{e}{16\pi^2 m^2_Z \sin 2\theta_W} 2\Delta T^{RL}_{3\psi mn} g^{mi*}_{l'R} g^{ni}_{lR} G_Z(m^2_{\psi_m}, m^2_{\psi_n}, m^2_{\phi_i}), \\ g^B_{RLRL} &= \frac{1}{16\pi^2} F(m^2_{\psi_m}, m^2_{\psi_n}, m^2_{\phi_i}, m^2_{\phi_j})(g^{mi*}_{l'R} g^{mj}_{lL} g^{nj*}_{l''R} g^{ni}_{lL} - 2\eta g^{mi*}_{l'R} g^{mj*}_{l''R} g^{ni}_{lL} g^{nj}_{lL}), \\ g^B_{RRRR} &= \frac{1}{16\pi^2} \left[\frac{\eta}{2} g^{mi*}_{l'R} g^{ni}_{lR} g^{mj*}_{l''R} g^{nj}_{lR} F(m^2_{\psi_m}, m^2_{\psi_n}, m^2_{\phi_i}, m^2_{\phi_j}) - \frac{1}{4} g^{mi*}_{l'R} g^{ni}_{lR} g^{nj*}_{l''R} g^{mj}_{lR} G(m^2_{\psi_m}, m^2_{\psi_n}, m^2_{\phi_i}, m^2_{\phi_j}) \right], \end{aligned}$$

$$g_{RRLL}^{B} = \frac{1}{16\pi^2}\left\{-\frac{1}{4}G(m_{\psi_m}^2, m_{\psi_n}^2, m_{\phi_i}^2, m_{\phi_j}^2)(g_{l'R}^{mi*}g_{lL}^{ni}g_{l''L}^{nj*}g_{lR}^{mj} + \eta g_{l'R}^{mi*}g_{lL}^{ni}g_{l''L}^{mj*}g_{lR}^{nj})\right.$$

$$-\frac{1}{2}g_{l'R}^{mi*}g_{lR}^{ni}g_{l''L}^{nj*}g_{lL}^{mj}F(m_{\psi_m}^2, m_{\psi_n}^2, m_{\phi_i}^2, m_{\phi_j}^2)$$

$$\left.+\frac{\eta}{4}g_{l'R}^{mi*}g_{lR}^{ni}g_{l''L}^{mj*}g_{lL}^{nj}G(m_{\psi_m}^2, m_{\psi_n}^2, m_{\phi_i}^2, m_{\phi_j}^2)\right\}, \tag{A11}$$

with

$$\kappa_{L(R)ijmn} \equiv \sin 2\theta_W(g_{l_{L(R)}}^Z\delta_{ij}\delta_{mn} - g_{\psi_{R(L)}mn}^Z\delta_{ij} - g_{\phi ij}^Z\delta_{mn})/2e,$$

$$\Delta T_{3\psi mn}^{RL} \equiv V_{mp}^R T_{3\psi_R p}V_{pn}^{\dagger L} - V_{mp}^L T_{3\psi_L p}V_{pn}^{\dagger R} \equiv \Delta T_{3\psi mn} = -\Delta T_{3\psi mn}^{LR}, \tag{A12}$$

$\eta = 1(0)$ for Majorana (Dirac) fermionic ψ and the loop functions $F_{(Z)}$ and $G_{(i,Z)}$ will be given shortly. Other g can be obtained by exchanging R and L. Note that $\Delta T_{3\psi}$ is basically the difference of weak isospin quantum numbers of ψ_R and ψ_L and in the case of no mixing, $\kappa_{L,R}$ are vanishing. Therefore, we expect $\Delta T_{3\psi}$ to be an order one quantity, while κ to be a much smaller quantity. Note that in case II the leading order contributions to the Z penguin amplitudes are at the level of $\delta_{LR}\delta_{RL}$, which is beyond the accuracy of the this analysis and their contributions are, hence, neglected.

The above loop functions are defined as [82]

$$F_1(a,b) = \frac{1}{12(a-b)^4}\left(2a^3 + 3a^2b - 6ab^2 + b^3 + 6a^2b\ln\frac{b}{a}\right),$$

$$F_2(a,b) = \frac{1}{2(a-b)^3}\left(-3a^2 + 4ab - b^2 - 2a^2\ln\frac{b}{a}\right),$$

$$F_3(a,b) = \frac{1}{2(a-b)^3}\left(a^2 - b^2 + 2ab\ln\frac{b}{a}\right),$$

$$G_1(a,b) = \frac{1}{36(a-b)^4}\left(-(a-b)(11a^2 - 7ab + 2b^2) - 6a^3\ln\frac{b}{a}\right),$$

$$G_2(a,b) = \frac{1}{36(a-b)^4}\left(-(a-b)(16a^2 - 29ab + 7b^2) - 6a^2(2a - 3b)\ln\frac{b}{a}\right),$$

$$G_3(a,b) = \frac{1}{36(a-b)^5}\left(-(a-b)(17a^2 + 8ab - b^2) - 6a^2(a + 3b)\ln\frac{b}{a}\right),$$

$$F_Z(a_1,a_2,b,b,c) = -\frac{a_1(2\sqrt{a_1a_2} - a_1)}{2(a_1-a_2)(a_1-b)}\ln\frac{a_1}{c} + \frac{a_2(2\sqrt{a_1a_2} - a_2)}{2(a_1-a_2)(a_2-b)}\ln\frac{a_2}{c} - \frac{b(2\sqrt{a_1a_2} - b)}{2(a_1-b)(a_2-b)}\ln\frac{b}{c},$$

$$F_Z(a,a,b_1,b_2,c) = -\frac{3}{4} + \frac{a^2}{2(a-b_1)(a-b_2)}\ln\frac{a}{c} - \frac{b_1^2}{2(a-b_1)(b_1-b_2)}\ln\frac{b_1}{c} + \frac{b_2^2}{2(a-b_2)(b_1-b_2)}\ln\frac{b_2}{c},$$

$$G_Z(a_1,a_2,b) = \frac{a_1\sqrt{a_1a_2}}{(a_1-a_2)(a_1-b)}\ln\frac{a_1}{b} - \frac{a_2\sqrt{a_1a_2}}{(a_1-a_2)(a_2-b)}\ln\frac{a_2}{b},$$

$$F(a,b,c,d) = \frac{b\sqrt{ab}}{(a-b)(b-c)(b-d)}\ln\frac{b}{a} - \frac{c\sqrt{ab}}{(a-c)(b-c)(c-d)}\ln\frac{c}{a} + \frac{d\sqrt{ab}}{(a-d)(b-d)(c-d)}\ln\frac{d}{a},$$

$$G(a,b,c,d) = -\frac{b^2}{(a-b)(b-c)(b-d)}\ln\frac{b}{a} + \frac{c^2}{(a-c)(b-c)(c-d)}\ln\frac{c}{a} - \frac{d^2}{(a-d)(b-d)(c-d)}\ln\frac{d}{a}. \tag{A13}$$

We do not need the generic expression of $F_Z(a_1, a_2, b_1, b_2, c)$, since only $a_1 = a_2 = a$ and/or $b_1 = b_2 = b$ are used in this work.

Comparing the generic expressions in Eq. (A5) to the following effective Lagrangians,

$$\mathcal{L}_{g-2} = -\frac{eQ}{4m_l}\Delta a_l \bar{l}\sigma_{\mu\nu}lF^{\mu\nu}, \qquad \mathcal{L}_{\text{EDM}} = -\frac{i}{2}d_l\bar{l}\sigma_{\mu\nu}\gamma_5 lF^{\mu\nu}, \tag{A14}$$

the Δa_l and d_l can be readily obtained as

$$\Delta a_l = -\frac{4m_l}{eQ_l}\text{Re}(A_{RL}), \qquad d_l = 2\text{Im}(A_{RL}). \qquad \text{(A15)}$$

The $\bar{l}' \to \bar{l}\gamma$ decay rate is related to the above $A_{M'N}$,

$$\Gamma(\bar{l}' \to \bar{l}\gamma) = \frac{(m_{l'}^2 - m_l^2)^3}{4\pi m_{l'}^3}(|A_{L'R}|^2 + |A_{R'L}|^2), \qquad \text{(A16)}$$

the $\bar{l}' \to \bar{l}l''\bar{l}$ decay rate is governed by the following formula, [19]

$$\Gamma(\bar{l}' \to \bar{l}l''\bar{l}) = \frac{m_{l'}^5}{3(8\pi)^3}\left[\frac{|g_{RLRL}|^2}{8} + 2|g_{RRRR}|^2 + |g_{RRLL}|^2 + 32\delta_{ll''}\left|\frac{eA_{R'L}}{m_{l'}}\right|^2\log\left(\frac{m_{l'}^2}{m_l^2} - \frac{11}{4}\right)\right.$$
$$\left. + 16\delta_{ll''}\text{Re}\left(\frac{eA_{R'L}g_{LLLL}^*}{m_{l'}}\right) + 8\delta_{ll''}\text{Re}\left(\frac{eA_{R'L}g_{LLRR}^*}{m_{l'}}\right)\right] + L \leftrightarrow R, \qquad \text{(A17)}$$

while the $l' \to l$ conversion rate ratio is given by

$$\mathcal{B}_{l'N \to eN} = \frac{\omega_{\text{conv}}}{\omega_{\text{capt}}}, \qquad \text{(A18)}$$

with

$$\omega_{\text{conv}} = \left|\frac{A_{R'L}^* D}{2m_{l'}} + 2[2g_{LV}^*(u) + g_{LV}^*(d)]V^{(p)} + 2[g_{LV}^*(u) + 2g_{LV}^*(d)]V^{(n)}\right|^2 + L \leftrightarrow R, \qquad \text{(A19)}$$

and the numerical values of D, V and ω_{capt} are taken from [85,86] and are collected in Table XII for completeness.

APPENDIX B: GAUGE QUANTUM NUMBERS OF ϕ AND ψ

The $\psi - \phi - l$ Lagrangian,

$$\mathcal{L}_{\text{int}} = g_L'(\bar{\psi}_R\phi_L^*)_i(L_L)_i + g_R'\bar{\psi}_L\phi_R^* l_R + \text{H.c.}, \qquad \text{(B1)}$$

where i is the weak isospin index, is gauge invariant under the SM gauge transformation. As the lepton quantum numbers under $SU(3) \times SU(2) \times U(1)$ are given by

$$L_L : \left(1, 2, -\frac{1}{2}\right), \qquad l_R : (1, 1, -1), \qquad \text{(B2)}$$

the gauge invariant requirement implies that we must have the following quantum number assignments for these combinations:

$$\bar{\psi}_R\phi_L^* : \left(1, 2, \frac{1}{2}\right), \qquad \bar{\psi}_L\phi_R^* : (1, 1, 1). \qquad \text{(B3)}$$

Consequently, the gauge quantum numbers of ψ and ϕ are related as follows:

TABLE XII. The overlap integrate parameters and total capture rates ω_{capt} taken from [85,86] are collected.

	$D(m_\mu^{5/2})$	$V^{(p)}(m_\mu^{5/2})$	$V^{(n)}(m_\mu^{5/2})$	$\omega_{\text{capt}}(10^6 s^{-1})$
$^{27}_{13}$Al	0.0362	0.0161	0.0173	0.7054
$^{48}_{22}$Ti	0.0864	0.0396	0.0468	2.59
$^{197}_{79}$Au	0.189	0.0974	0.146	13.07
$^{205}_{81}$Tl	0.161	0.0834	0.128	13.90

$$\psi_R : (c_R, 2I_R + 1, Y_R),$$
$$\phi_L : (\bar{c}_R, 2(I_R \pm 1/2) + 1, Y_R - 1/2),$$
$$\psi_L : (c_L, 2I_L + 1, Y_L), \qquad \phi_R : (\bar{c}_L, 2I_L + 1, Y_L - 1). \qquad \text{(B4)}$$

Some examples of the assignments of the quantum numbers of $\psi_{L,R}$ and $\phi_{L,R}$ are given in Table XIII.

As discussed in the main text chiral enhancement in photonic dipole penguins is an important ingredient to general sizable Δa_μ and Δa_e. To have chiral enhancement one needs to connect ϕ_L and ϕ_R by Higgs VEV with ψ_R and ψ_L having identical quantum numbers or the other way around, see Fig. 2 and the related discussion. There are four possibilities on the quantum numbers of the $\bar{\psi}_L\psi_R$ and $\phi_L^*\phi_R$ combinations to achieve that:

TABLE XIII. Some examples of the assignment of the quantum numbers of $\psi_{L,R}$ and $\phi_{L,R}$.

ψ_R	ϕ_L	ψ_L	ϕ_R
$(1, 1, Y_R)$	$(1, 2, Y_R - \frac{1}{2})$	$(1, 1, Y_L)$	$(1, 1, Y_L - 1)$
$(1, 2, Y_R)$	$(1, 1, Y_R - \frac{1}{2})$	$(1, 2, Y_L)$	$(1, 2, Y_L - 1)$
$(3(\bar{3}), 1, Y_R)$	$(\bar{3}(3), 2, Y_R - \frac{1}{2})$	$(3(\bar{3}), 1, Y_L)$	$(\bar{3}(3), 1, Y_L - 1)$
$(3(\bar{3}), 2, Y_R)$	$(\bar{3}(3), 1, Y_R - \frac{1}{2})$	$(3(\bar{3}), 2, Y_L)$	$(\bar{3}(3), 2, Y_L - 1)$

TABLE XIV. Some examples of the assignment of the quantum numbers of $\psi_{L,R}$ and $\phi_{L,R}$ that can generate chiral enhancement in photonic dipole penguins.

Case	ψ_R	ϕ_L	ψ_L	ϕ_R
(A)	$(1,1,Y)$	$(1,2,Y-\frac{1}{2})$	$(1,1,Y)$	$(1,1,Y-1)$
(A)	$(1,2,Y)$	$(1,1,Y-\frac{1}{2})$	$(1,2,Y)$	$(1,2,Y-1)$
(A)	$(3(\bar{3}),1,Y)$	$(\bar{3}(3),2,Y-\frac{1}{2})$	$(3(\bar{3}),1,Y)$	$(\bar{3}(3),1,Y-1)$
(A)	$(3(\bar{3}),2,Y)$	$(\bar{3}(3),1,Y-\frac{1}{2})$	$(3(\bar{3}),2,Y)$	$(\bar{3}(3),2,Y-1)$
(C)	$(1,1,Y-\frac{1}{2})$	$(1,2,Y-1)$	$(1,2,Y)$	$(1,2,Y-1)$
(C)	$(1,2,Y-\frac{1}{2})$	$(1,1,Y-1)$	$(1,1,Y)$	$(1,1,Y-1)$
(C)	$(3(\bar{3}),1,Y-\frac{1}{2})$	$(\bar{3}(3),2,Y-1)$	$(3(\bar{3}),2,Y)$	$(\bar{3}(3),2,Y-1)$
(C)	$(3(\bar{3}),2,Y-\frac{1}{2})$	$(\bar{3}(3),1,Y-1)$	$(3(\bar{3}),1,Y)$	$(\bar{3}(3),1,Y-1)$

$$
\begin{aligned}
(A)&: \bar{\psi}_L\psi_R:(1,1,0), \qquad \phi_L^*\phi_R:(1,2,-1/2), \\
(B)&: \bar{\psi}_L\psi_R:(1,1,0), \qquad \phi_L^*\phi_R:(1,2,+1/2), \\
(C)&: \bar{\psi}_L\psi_R:(1,2,-1/2), \qquad \phi_L^*\phi_R:(1,1,0), \\
(D)&: \bar{\psi}_L\psi_R:(1,2,+1/2), \qquad \phi_L^*\phi_R:(1,1,0).
\end{aligned} \tag{B5}
$$

The above equation imposes additional constraints on the quantum numbers of the new fields:

$$
\begin{aligned}
(A)&: c_R=c_L, \quad I_R=I_L, \quad Y_R=Y_L, \quad -Y_R+\frac{1}{2}+Y_L-1=-\frac{1}{2}, \\
(B)&: c_R=c_L, \quad I_R=I_L, \quad Y_R=Y_L, \quad -Y_R+\frac{1}{2}+Y_L-1=+\frac{1}{2}, \\
(C)&: c_R=c_L, \quad I_R\pm\frac{1}{2}=I_L, \quad -Y_L+Y_R=-\frac{1}{2}, \quad -Y_R+\frac{1}{2}+Y_L-1=0, \\
(D)&: c_R=c_L, \quad I_R\pm\frac{1}{2}=I_L, \quad -Y_L+Y_R=+\frac{1}{2}, \quad -Y_R+\frac{1}{2}+Y_L-1=0,
\end{aligned} \tag{B6}
$$

where use of Eq. (B4) has been made.

One can easily see that cases (B) and (D) are invalid as there are no solutions satisfying their conditions, and we are left with cases (A) and (C). In case (A), ψ_L and ψ_R have identical quantum numbers, while ϕ_L and ϕ_R are mixed via the Higgs VEV. By contrast, in case (C), ϕ_L and ϕ_R have identical quantum numbers, while ψ_L and ψ_R are mixed via

the Higgs VEV. To generate chiral enhancement in photonic penguins, case (A) is in general more preferable as the mass of ψ is not limited by the Higgs VEV and the Yukawa coupling.

In Table XIV, we give some samples of the assignment of the quantum numbers of the new fields that can generate chiral enhancement in photonic dipole penguins.

[1] I. Melzer-Pellmann, Searches for supersymmetry, Proc. Sci., EPS-HEP2019 (**2019**) 710; M. H. Genest, Searches for exotica, Proc. Sci., EPS-HEP2019 (**2019**) 721.

[2] H. N. Brown *et al.* (Muon $g-2$ Collaboration), Precise Measurement of the Positive Muon Anomalous Magnetic Moment, Phys. Rev. Lett. **86**, 2227 (2001).

[3] G. W. Bennett *et al.* (Muon $g-2$ Collaboration), Final report of the muon E821 anomalous magnetic moment measurement at BNL, Phys. Rev. D **73**, 072003 (2006).

[4] M. Tanabashi *et al.* (Particle Data Group), Review of particle physics, Phys. Rev. D **98**, 030001 (2018).

[5] A. Keshavarzi, D. Nomura, and T. Teubner, Muon $g-2$ and $\alpha(M_Z^2)$: A new data-based analysis, Phys. Rev. D **97**, 114025 (2018).

[6] F. Jegerlehner and A. Nyffeler, The Muon $g-2$, Phys. Rep. **477**, 1 (2009).

[7] M. Davier, A. Hoecker, B. Malaescu, and Z. Zhang, Reevaluation of the hadronic contributions to the muon

$g - 2$ and to alpha(MZ), Eur. Phys. J. C **71**, 1515 (2011); Reevaluation of the hadronic vacuum polarisation contributions to the Standard Model predictions of the muon $g - 2$ and $\alpha(m_Z^2)$ using newest hadronic cross-section data, Eur. Phys. J. C **77**, 827 (2017); A new evaluation of the hadronic vacuum polarisation contributions to the muon anomalous magnetic moment and to $\boldsymbol{\alpha(m_Z^2)}$, Eur. Phys. J. C **80**, 241 (2020).

[8] F. Campanario, H. Czy, J. Gluza, T. Jeliski, G. Rodrigo, S. Tracz, and D. Zhuridov, Standard model radiative corrections in the pion form factor measurements do not explain the a_μ anomaly, Phys. Rev. D **100**, 076004 (2019).

[9] T. Aoyama *et al.*, The anomalous magnetic moment of the muon in the Standard Model, arXiv:2006.04822.

[10] G. Venanzoni (Fermilab E989 Collaboration), The New Muon $g - 2$ experiment at Fermilab, Nucl. Part. Phys. Proc. **273–275**, 584 (2016); J-PARC E34 experiment web page, (http://g-2.kek.jp/portal/index.html).

[11] R. H. Parker, C. Yu, W. Zhong, B. Estey, and H. Mller, Measurement of the fine-structure constant as a test of the Standard Model, Science **360**, 191 (2018).

[12] S. Eidelman and M. Passera, Theory of the tau lepton anomalous magnetic moment, Mod. Phys. Lett. A **22**, 159 (2007).

[13] T. Fukuyama, Searching for new physics beyond the standard model in electric dipole moment, Int. J. Mod. Phys. A **27**, 1230015 (2012).

[14] V. Andreev *et al.* (ACME Collaboration), Improved limit on the electric dipole moment of the electron, Nature (London) **562**, 355 (2018).

[15] G. W. Bennett *et al.* (Muon $(g - 2)$ Collaboration), An improved limit on the muon electric dipole moment, Phys. Rev. D **80**, 052008 (2009).

[16] A. G. Grozin, I. B. Khriplovich, and A. S. Rudenko, Electric dipole moments, from e to tau, Phys. At. Nucl. **72**, 1203 (2009).

[17] A. M. Baldini *et al.* (MEG Collaboration), Search for the lepton flavour violating decay $\mu^+ \to e^+\gamma$ with the full dataset of the MEG experiment, Eur. Phys. J. C **76**, 434 (2016).

[18] A. M. Baldini *et al.* (MEG II Collaboration), The design of the MEG II experiment, Eur. Phys. J. C **78**, 380 (2018).

[19] Y. Kuno and Y. Okada, Muon decay and physics beyond the standard model, Rev. Mod. Phys. **73**, 151 (2001).

[20] M. Lindner, M. Platscher, and F. S. Queiroz, A call for new physics: The muon anomalous magnetic moment and lepton flavor violation, Phys. Rep. **731**, 1 (2018).

[21] Z. Berezhiani and M. Khlopov, Cosmology of spontaneously broken gauge family symmetry, Z. Phys. C **49**, 73 (1991).

[22] Y. Amhis *et al.* (HFLAV Collaboration), Averages of *b*-hadron, *c*-hadron, and *τ*-lepton properties as of summer 2016, Eur. Phys. J. C **77**, 895 (2017).

[23] E. Kou *et al.* (Belle-II Collaboration), The Belle II physics book, Prog. Theor. Exp. Phys. **2019**, 123C01 (2019); Erratum, **2020**, 029201 (2020).

[24] S. Mihara, cLFV/g-2/EDM experiments, Proc. Sci. ICHEP2018 (**2018**) 714.

[25] H. Davoudiasl and W. J. Marciano, Tale of two anomalies, Phys. Rev. D **98**, 075011 (2018).

[26] A. Berlin, N. Blinov, G. Krnjaic, P. Schuster, and N. Toro, Dark matter, millicharges, axion and scalar particles, gauge bosons, and other new physics with LDMX, Phys. Rev. D **99**, 075001 (2019).

[27] A. Crivellin, M. Hoferichter, and P. Schmidt-Wellenburg, Combined explanations of $(g - 2)_{\mu,e}$ and implications for a large muon EDM, Phys. Rev. D **98**, 113002 (2018).

[28] J. X. Pan, M. He, X. G. He, and G. Li, Scrutinizing a massless dark photon: Basis independence, Nucl. Phys. **B953**, 114968 (2020).

[29] W. Dekens, E. E. Jenkins, A. V. Manohar, and P. Stoffer, Non-perturbative effects in $\mu \to e\gamma$, J. High Energy Phys. 01 (2019) 088.

[30] J. Liu, C. E. M. Wagner, and X. P. Wang, A light complex scalar for the electron and muon anomalous magnetic moments, J. High Energy Phys. 03 (2019) 008.

[31] B. Dutta and Y. Mimura, Electron $g - 2$ with flavor violation in MSSM, Phys. Lett. B **790**, 563 (2019).

[32] X. F. Han, T. Li, L. Wang, and Y. Zhang, Simple interpretations of lepton anomalies in the lepton-specific inert two-Higgs-doublet model, Phys. Rev. D **99**, 095034 (2019).

[33] R. Coy and M. Frigerio, Effective approach to lepton observables: The seesaw case, Phys. Rev. D **99**, 095040 (2019).

[34] X. X. Dong, S. M. Zhao, H. B. Zhang, and T. F. Feng, The two-loop corrections to lepton MDMs and EDMs in the EBLMSSM, J. Phys. G **47**, 045002 (2020).

[35] C. R. Chen, C. W. Chiang, and K. Y. Lin, A variant two-Higgs doublet model with a new Abelian gauge symmetry, Phys. Lett. B **795**, 22 (2019).

[36] G. Mohlabeng, Revisiting the dark photon explanation of the muon anomalous magnetic moment, Phys. Rev. D **99**, 115001 (2019).

[37] M. Ibe, M. Suzuki, T. T. Yanagida, and N. Yokozaki, Muon $g - 2$ in split-family SUSY in light of LHC run II, Eur. Phys. J. C **79**, 688 (2019).

[38] A. E. Crcamo Hernndez, J. Marchant Gonzlez, and U. J. Saldaa-Salazar, Viable low-scale model with universal and inverse seesaw mechanisms, Phys. Rev. D **100**, 035024 (2019).

[39] A. Crivellin and M. Hoferichter, Combined explanations of $(g - 2)_\mu$, $(g - 2)_e$ and implications for a large muon EDM, arXiv:1905.03789.

[40] K. Harigaya, R. Mcgehee, H. Murayama, and K. Schutz, A predictive mirror twin Higgs with small Z_2 breaking, J. High Energy Phys. 05 (2020) 155.

[41] I. Bigaran, J. Gargalionis, and R. R. Volkas, A near-minimal leptoquark model for reconciling flavour anomalies and generating radiative neutrino masses, J. High Energy Phys. 10 (2019) 106.

[42] M. Endo and W. Yin, Explaining electron and muon $g - 2$ anomaly in SUSY without lepton-flavor mixings, J. High Energy Phys. 08 (2019) 122.

[43] J. Kawamura, S. Raby, and A. Trautner, Complete vectorlike fourth family and new $U(1)'$ for muon anomalies, Phys. Rev. D **100**, 055030 (2019).

[44] M. Abdullah, B. Dutta, S. Ghosh, and T. Li, $(g - 2)_{\mu,e}$ and the ANITA anomalous events in a three-loop neutrino mass model, Phys. Rev. D **100**, 115006 (2019).

[45] M. Bauer, M. Neubert, S. Renner, M. Schnubel, and A. Thamm, Axion-Like Particles, Lepton-Flavor Violation and A New Explanation of a_μ and a_e, Phys. Rev. Lett. **124,** 211803 (2020).

[46] M. Badziak and K. Sakurai, Explanation of electron and muon $g-2$ anomalies in the MSSM, J. High Energy Phys. 10 (2019) 024.

[47] R. Mandal and A. Pich, Constraints on scalar leptoquarks from lepton and kaon physics, J. High Energy Phys. 12 (2019) 089.

[48] A. E. Cárcamo Hernández, S. F. King, H. Lee, and S. J. Rowley, Is it possible to explain the muon and electron $g-2$ in a $Z\prime$ model?, Phys. Rev. D **101,** 115016 (2020).

[49] A. E. Cárcamo Hernández, D. T. Huong, and H. N. Long, A minimal model for the SM fermion flavor structure, mass hierarchy, dark matter, leptogenesis and the $g-2$ anomalies, Phys. Rev. D **102,** 055002 (2020).

[50] G. Hiller, C. Hormigos-Feliu, D. F. Litim, and T. Steudtner, Anomalous magnetic moments from asymptotic safety, arXiv:1910.14062.

[51] A. Keshavarzi, D. Nomura, and T. Teubner, $g-2$ of charged leptons, $\alpha(M_Z^2)$, and the hyperfine splitting of muonium, Phys. Rev. D **101,** 014029 (2020).

[52] J. Bramante and E. Gould, Anomalous anomalies from virtual black holes, Phys. Rev. D **101,** 055007 (2020).

[53] C. Cornella, P. Paradisi, and O. Sumensari, Hunting for ALPs with lepton flavor violation, J. High Energy Phys. 01 (2020) 158.

[54] J. Kawamura, S. Raby, and A. Trautner, Complete vectorlike fourth family with $U(1)\prime$: A global analysis, Phys. Rev. D **101,** 035026 (2020).

[55] L. Calibbi, T. Li, Y. Li, and B. Zhu, Simple model for large CP violation in charm decays, B-physics anomalies, muon $g-2$, and Dark Matter, arXiv:1912.02676.

[56] N. V. Krasnikov, Implications of last NA64 results and the electron g_e-2 anomaly for the X(16.7) boson survival, Mod. Phys. Lett. A **35,** 2050116 (2020).

[57] W. Altmannshofer, S. Gori, H. H. Patel, S. Profumo, and D. Tuckler, Electric dipole moments in a leptoquark scenario for the B-physics anomalies, J. High Energy Phys. 05 (2020) 069.

[58] M. Endo, S. Iguro, and T. Kitahara, Probing $e\mu$ flavor-violating ALP at Belle II, J. High Energy Phys. 06 (2020) 040.

[59] A. E. Crcamo Hernndez, Y. Hidalgo Velsquez, S. Kovalenko, H. N. Long, N. A. Prez-Julve, and V. V. Vien, Fermion spectrum and $g-2$ anomalies in a low scale 3-3-1 model, arXiv:2002.07347.

[60] N. Haba, Y. Shimizu, and T. Yamada, Muon and electron $g-2$ and the origin of fermion mass hierarchy, arXiv:2002.10230.

[61] W. Altmannshofer, P. S. B. Dev, A. Soni, and Y. Sui, Addressing R$_{D^{(*)}}$, R$_{K^{(*)}}$, muon $g-2$ and ANITA anomalies in a minimal R-parity violating supersymmetric framework, Phys. Rev. D **102,** 015031 (2020).

[62] I. Bigaran and R. R. Volkas, Getting chirality right: Single scalar leptoquark solutions to the $(g-2)_{e,\mu}$ puzzle, arXiv:2002.12544.

[63] S. Jana, Vishnu P. K., and S. Saad, Resolving electron and muon $g-2$ within the 2HDM, Phys. Rev. D **101,** 115037 (2020).

[64] L. Calibbi, M. L. Lpez-Ibez, A. Melis, and O. Vives, Muon and electron $g-2$ and lepton masses in flavor models, J. High Energy Phys. 06 (2020) 087.

[65] C. H. Chen and T. Nomura, Electron and muon $g-2$, radiative neutrino mass, and $\ell\prime \to \ell\gamma$ in a $U(1)_{e-\mu}$ model, arXiv:2003.07638.

[66] J. L. Yang, T. F. Feng, and H. B. Zhang, Electron and muon $(g-2)$ in the B-LSSM, J. Phys. G **47,** 055004 (2020).

[67] C. Hati, J. Kriewald, J. Orloff, and A. M. Teixeira, Anomalies in ^{8}Be nuclear transitions and $(g-2)_{e,\mu}$: Towards a minimal combined explanation, J. High Energy Phys. 07 (2020) 235.

[68] M. Frank, Y. Hiylmaz, S. Moretti, and Ö. Özdal, Leptophobic $Z\prime$ bosons in the secluded $U(1)\prime$ model, arXiv: 2005.08472.

[69] B. Dutta, S. Ghosh, and T. Li, Explaining $(g-2)_{\mu,e}$, KOTO anomaly and MiniBooNE excess in an extended Higgs model with sterile neutrinos, arXiv:2006.01319.

[70] F. J. Botella, F. Cornet-Gomez, and M. Nebot, Electron and muon $g-2$ anomalies in general flavour conserving two Higgs doublets models, Phys. Rev. D **102,** 035023 (2020).

[71] W. Abdallah, R. Gandhi, and S. Roy, Understanding the MiniBooNE and the muon $g-2$ anomalies with a light $Z\prime$ and a second Higgs doublet, arXiv:2006.01948.

[72] K. F. Chen, C. W. Chiang, and K. Yagyu, An explanation for the muon and electron $g-2$ anomalies and dark matter, arXiv:2006.07929.

[73] I. Dorner, S. Fajfer, and S. Saad, $\mu \to e\gamma$ selecting scalar leptoquark solutions for the $(g-2)_{e,\mu}$ puzzles, arXiv: 2006.11624.

[74] A. Keshavarzi, W. J. Marciano, M. Passera, and A. Sirlin, The muon $g-2$ and $\Delta\alpha$ connection, Phys. Rev. D **102,** 033002 (2020).

[75] C. Arbelez, R. Cepedello, R. M. Fonseca, and M. Hirsch, $(g-2)$ anomalies and neutrino mass, arXiv:2007.11007.

[76] T. Nomura, H. Okada, and Y. Uesaka, A two-loop induced neutrino mass model, dark matter, and LFV processes $\ell_i \to \ell_j\gamma$, and $\mu e \to ee$ in a hidden local $U(1)$ symmetry, arXiv:2008.02673.

[77] S. Jana, P. K. Vishnu, W. Rodejohann, and S. Saad, Dark matter assisted lepton anomalous magnetic moments and neutrino masses, arXiv:2008.02377.

[78] V. Gherardi, D. Marzocca, and E. Venturini, Low-energy phenomenology of scalar leptoquarks at one-loop accuracy, arXiv:2008.09548.

[79] Y. Kuno and Y. Okada, Muon decay and physics beyond the standard model, Rev. Mod. Phys. **73,** 151 (2001).

[80] A. Crivellin, S. Najjarim, and J. Rosiek, Lepton flavor violation in the standard model with general dimension-six operators, J. High Energy Phys. 04 (2014) 167.

[81] W. Buchmuller and D. Wyler, Effective Lagrangian analysis of new interactions and flavor Conservation, Nucl. Phys. **B268,** 621 (1986).

[82] C. K. Chua, Implications of Br$(\mu \to e\gamma)$ and Δa_μ on muonic lepton flavor violating processes, Phys. Rev. D **86,** 093009 (2012).

[83] P. Arnan, L. Hofer, F. Mescia, and A. Crivellin, Loop effects of heavy new scalars and fermions in $b \to s\mu^+\mu^-$, J. High Energy Phys. 04 (2017) 043.

[84] F. Gabbiani, E. Gabrielli, A. Masiero, and L. Silvestrini, A complete analysis of FCNC and *CP* constraints in general SUSY extensions of the standard model, Nucl. Phys. **B477,** 321 (1996).

[85] R. Kitano, M. Koike, and Y. Okada, Detailed calculation of lepton flavor violating muon electron conversion rate for various nuclei, Phys. Rev. D **66,** 096002 (2002); Erratum, **76,** 059902 (2007).

[86] T. Suzuki, D. F. Measday, and J. P. Roalsvig, Total nuclear capture rates for negative muons, Phys. Rev. C **35,** 2212 (1987).